gebiology

Geobiology (2016), **14**, 344–363 DOI: 10.1111/gbi.12178

Environmental context for the terminal Ediacaran biomineralization of animals

H. CUI,[1,2] A. J. KAUFMAN,[1,3] S. XIAO,[4] S. PEEK,[1,*] H. CAO,[1,†] X. MIN,[5] Y. CAI,[5] Z. SIEGEL,[6] X.-M. LIU,[7] Y. PENG,[8] J. D. SCHIFFBAUER[9] AND A. J. MARTIN[10]

[1]*Department of Geology, University of Maryland, College Park, MD, USA*
[2]*Department of Geoscience and NASA Astrobiology Institute, University of Wisconsin-Madison, Madison, WI, USA*
[3]*Earth System Science Interdisciplinary Center, University of Maryland, College Park, MD, USA*
[4]*Department of Geosciences, Virginia Tech, Blacksburg, VA, USA*
[5]*Department of Geology, Northwest University, Xi'an, China*
[6]*Bethesda-Chevy Chase High School, Bethesda, MD, USA*
[7]*Department of Geological Sciences, University of North Carolina, Chapel Hill, NC, USA*
[8]*Department of Geology and Geophysics, Louisiana State University, Baton Rouge, LA, USA*
[9]*Department of Geological Sciences, University of Missouri, Columbia, MO, USA*
[10]*División de Geociencias Aplicadas, IPICYT, San Luis Potosí, Mexico*

ABSTRACT

In terminal Ediacaran strata of South China, the onset of calcareous biomineralization is preserved in the paleontological transition from *Conotubus* to *Cloudina* in repetitious limestone facies of the Dengying Formation. Both fossils have similar size, funnel-in-funnel construction, and epibenthic lifestyle, but *Cloudina* is biomineralized, whereas *Conotubus* is not. To provide environmental context for this evolutionary milestone, we conducted a high-resolution elemental and stable isotope study of the richly fossiliferous Gaojiashan Member. Coincident with the first appearance of *Cloudina* is a significant positive carbonate carbon isotope excursion (up to +6‰) and an increase in the abundance and ^{34}S composition of pyrite. In contrast, $\delta^{34}S$ values of carbonate-associated sulfate remain steady throughout the succession, resulting in anomalously large (>70‰) sulfur isotope fractionations in the lower half of the member. The fractionation trend likely relates to changes in microbial communities, with sulfur disproportionation involved in the lower interval, whereas microbial sulfate reduction was the principal metabolic pathway in the upper. We speculate that the coupled paleontological and biogeochemical anomalies may have coincided with an increase in terrestrial weathering fluxes of sulfate, alkalinity, and nutrients to the depositional basin, which stimulated primary productivity, the spread of an oxygen minimum zone, and the development of euxinic conditions in subtidal and basinal environments. Enhanced production and burial of organic matter is thus directly connected to the carbon isotope anomaly, and likely promoted pyritization as the main taphonomic pathway for *Conotubus* and other soft-bodied Ediacara biotas. Our studies suggest that the Ediacaran confluence of ecological pressures from predation and environmental pressures from an increase in seawater alkalinity set the stage for an unprecedented geobiological response: the evolutionary novelty of animal biomineralization.

Received 02 October 2015; accepted 19 January 2016

Corresponding author: H. Cui. Tel.: +1 240 281 1865; fax: +1 608 262 0693; e-mail: Huan.Cui@wisc.edu

*Present address: United States Geological Survey, Menlo Park, CA 94025, USA

†Present address: College of Earth Sciences, Jilin University, Changchun 130061, China

INTRODUCTION

One of the earliest animals to have developed a biomineralized carbonate exoskeleton is *Cloudina*—named after the famed Precambrian paleontologist Preston Cloud (1912–1991) and preserved in terminal Ediacaran (ca. 550–541 Ma) sedimentary successions worldwide (Conway Morris *et al.*, 1990; Sour-Tovar *et al.*, 2007;

Gaucher & Germs, 2009; Cortijo *et al.*, 2010; Zhuravlev *et al.*, 2012). This animal, which is suggested to be an ancient cnidarian-grade (Grant, 1992; Cortijo *et al.*, 2010) or lophotrochozoan animal (Hua *et al.*, 2005; Zhuravlev *et al.*, 2015), constructed a high-Mg calcitic tubular shell with nested funnels, had an epibenthic lifestyle with its apex attached to the substrate (Grant, 1990; Zhuravlev *et al.*, 2012; Cai *et al.*, 2014), and may have had both sexual and asexual reproductive strategies to aid in its broad ecological dispersal (Cortijo *et al.*, 2015). *Cloudina* was associated with microbial reefs and may have been a reef builder like modern-day corals that inhabit oligotrophic shelf environments where they band together in search of hard substrates and for protection against predators (Penny *et al.*, 2014; Wood & Curtis, 2015).

Biomineralization of *Cloudina* is widely considered to have been a response to predation given the significant number of borings found on its fossil shells (Bengtson & Zhao, 1992; Hua *et al.*, 2003; Porter, 2011). In addition, some also have considered terminal Ediacaran biomineralization as a (toxico-)physiological response to regulate calcium concentrations in circulatory fluids (Simkiss, 1977, 1989; Kempe *et al.*, 1989; Brennan *et al.*, 2004), or to environmental perturbations involving oscillations in atmospheric pCO_2 and seawater chemistry (Knoll, 2003a; Knoll & Fischer, 2011). Environmental drivers, however, are particularly difficult to assess insofar as these should also have a broad effect on general biotic diversification and vice versa (Knoll, 2003b; Gaidos *et al.*, 2007; Butterfield, 2009, 2011; Lenton *et al.*, 2014; Erwin, 2015). Insofar as there is a metabolic cost to biomineralization, the biological benefits to the organisms, including protection against predation and the physiological response of organisms to rapidly changing seawater chemistry in the terminal Ediacaran Period, should be balanced (Knoll, 2003a; Xiao, 2014).

To this end, we investigated a Lagerstätte of Ediacaran animals in the Gaojiashan Member of the Dengying Formation in South China (Fig. 1) (Hua *et al.*, 2007; Cai *et al.*, 2010). Within the member's repetitious limestone facies, the first appearance of *Cloudina* is immediately preceded by *Conotubus*, a soft-bodied antecedent exquisitely preserved through pyritization with similar construction, size, and lifestyle (Cai *et al.*, 2011, 2014). To explore this unique paleontological juxtaposition and provide environmental context for the earliest examples of animal biomineralization and pyritization, we sampled the Gaojiashan Member at high stratigraphic resolution for elemental and isotopic compositions. Our chemostratigraphic investigation reveals that these evolutionary and taphonomic events are associated with profound biogeochemical shifts in both the carbon and sulfur cycles, and speculate that they may have been facilitated by profound environmental perturbations in the marine realm ultimately driven by enhanced oxidative weathering of the continents.

STRATIGRAPHIC AND GEOCHRONOLOGICAL CONSTRAINTS

Carbonates of the Dengying platform are sandwiched between the Ediacaran Doushantuo Formation (ca. 635–551 Ma) (Jiang *et al.*, 2011) and the early Cambrian Kuanchuanpu Formation (Steiner *et al.*, 2004) in the southern Shaanxi region (Fig. 1). The Dengying Formation at Gaojiashan is subdivided into three intervals, including the Algal Dolomite, Gaojiashan, and Beiwan members (Fig. 1C), which are generally correlated with Hamajing, Shibantan, and Baimatuo members, respectively, in the Yangtze Gorges area (Zhou & Xiao, 2007; Zhu *et al.*, 2007; Duda *et al.*, 2015). Based on the 551 Ma U-Pb zircon depositional age of a volcanic ash at the top of the Miaohe Member, which has historically been correlated with Doushantuo Member IV (Condon *et al.*, 2005), and an estimated 541 Ma age for the Ediacaran–Cambrian boundary (Amthor *et al.*, 2003; Chen *et al.*, 2015), the >650 m thick Dengying Formation represents the last 10 million years of the Ediacaran Period. However, a recent chemostratigraphic study of the Miaohe Member (An *et al.*, 2015) demonstrates that the 551 Ma ash bed lies between the Hamajing and Shibantan members of the Dengying Formation and is thus not relevant to the biogeochemical anomaly (i.e., Shuram excursion) preserved in the upper Doushantuo Formation (*cf.* Kaufman, 2005).

At the studied section, the Gaojiashan Member is 55 m in thickness, including a siltstone interval in the lower part, repetitious siltstone–mudstone–limestone facies with cryptalgal crinkly laminations in the middle part, and a coarse sandstone/conglomerate at the top (Fig. 2) (Cai *et al.*, 2010). The lower Gaojiashan Member contains the enigmatic fossil *Shaanxilithes ningqiangensis* preserved in siltstone facies (Meyer *et al.*, 2012). The middle Gaojiashan Member contains *Conotubus hemiannulatus* and *Gaojiashania cyclus* preserved in thin, normally graded calcisiltite–siltstone beds interpreted as distal event deposits (Cai *et al.*, 2010), followed by the first appearance of the biomineralized animal *Cloudina* preserved in intraclastic limestones approximately 40 m above the base of the succession (Fig. 1). A distinctive horizon with bedded gypsum occurs in the upper part of the Gaojiashan Member (Figs 1D, 2F,G).

METHODS

In this study, the Gaojiashan Member was systematically sampled at high resolution for integrated chemostratigraphic and geochronological investigations. Geochemical analyses were conducted in the Paleoclimate CoLaboratory at University of Maryland. Details of the methods used in the CoLaboratory can be found in previous publications (e.g., McFadden *et al.*, 2008; Zhelezinskaia *et al.*, 2014; Cui *et al.*, 2015), but are briefly outlined below.

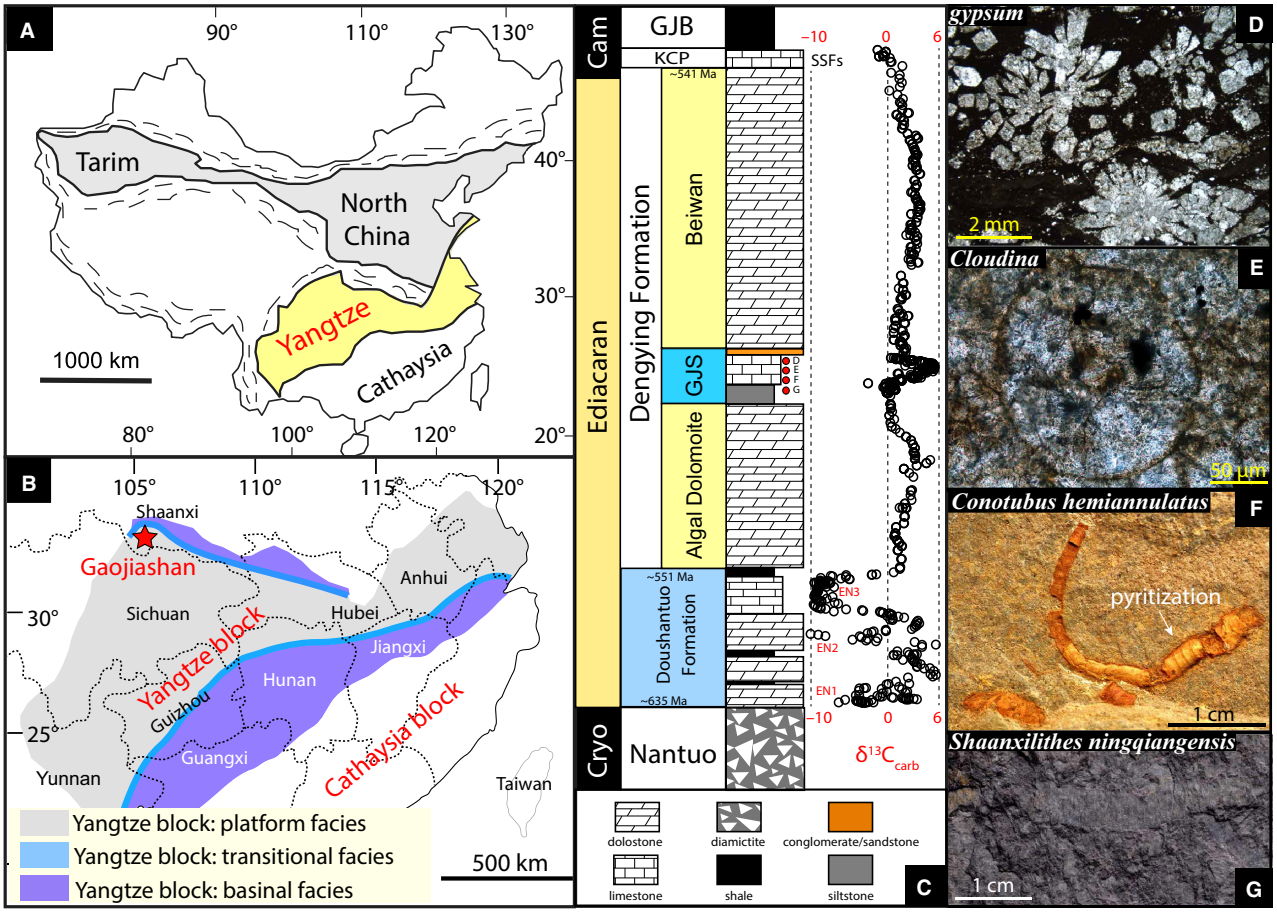

Fig. 1 (A) Tectonic framework of China, with the Yangtze Craton highlighted in yellow. (B) Ediacaran depositional environments on the Yangtze Craton (Jiang *et al.*, 2011). (C) $\delta^{13}C_{carb}$ record of the Dengying Formation in the Gaojiashan section. GJS = Gaojiashan, KCP = Kuanchuanpu, GJB = Guojiaba, Cryo = Cryogenian, Cam = Cambrian; $\delta^{13}C_{carb}$ data for Doushantuo Formation are from McFadden *et al.* (2008). (D) Calcite pseudomorph after gypsum ca. 46.5 m above the base of the Gaojiashan Member. (E) *Cloudina* in the Gaojiashan Member ca. 42 m above the base. (F) Pyritized tubular fossil *Conotubus hemiannulatus* (Cai *et al.*, 2011). (G) Enigmatic body fossil *Shaanxilithes ningqiangensis* (Meyer *et al.*, 2012).

Carbon and oxygen isotope analysis

Rock samples were cut and polished for detailed petrographic observation and micro-drilling to obtain powders from the least-altered, least-recrystallized, and purest phases for carbonate carbon ($\delta^{13}C_{carb}$) and oxygen ($\delta^{18}O_{carb}$) isotope analysis. The powders were measured with a Multicarb inlet device in-line with an Elementar Isoprime continuous-flow isotope ratio mass spectrometer, and precision for both isotopes was routinely better than 0.1‰.

Elemental analyses

Major and trace elemental abundances in carbonates were analyzed to better evaluate the degree of diagenetic alteration. Aliquots of the micro-drilled carbonate powders were dissolved in 0.4 M HNO_3 and centrifuged. The purified solutions were isolated prior to analysis. Petrographic observations indicate that these powders were largely free of siliciclastics; any clays, if present, would not have been dissolved by the dilute acid. The resulting solutions were analyzed on a Thermo Scientific® (Waltham, MA, USA) iCAP-Q ICP-MS (Inductively Coupled Plasma—Mass Spectrometry) at the Carnegie Institution of Washington. Precision of these analyses as determined by repeated measurements of a house standard carbonate was <5% (2σ) for major elements with high concentrations and <10% (2σ) for the REEs.

Organic carbon and paired sulfur isotope analyses

The organic carbon ($\delta^{13}C_{org}$), total sulfur ($\delta^{34}S_{TS}$ of pyrite and trace amount of organic S) isotope compositions were measured by combustion of the decalcified residuals to CO_2 or SO_2 with a Eurovector elemental analyzer in-line with a second Elementar Isoprime isotope ratio mass spectrometer. Bulk carbonate powders were used for extraction

of carbonate-associated sulfate (CAS). For the former, ~15 g of bulk crushed sample was acidified with 3 M HCl. These acidified residues were washed with ultra-pure Milli-Q (18 MΩ) water, centrifuged, decanted, and dried. For the latter, ~100 g of crushed bulk sample were repeatedly leached with 10% NaCl solutions. To minimize the contamination of soluble non-CAS sulfate (Marenco *et al.*, 2008; Wotte *et al.*, 2012; Peng *et al.*, 2014; Schobben *et al.*, 2015), bulk powders were leached with 10% NaCl solutions for at least 10 times (~2 h each), and then washed with Milli-Q water for at least three times prior to acidification of the leached powders with 3 M HCl. CAS precipitates were then collected as $BaSO_4$ three days after $BaCl_2$ was added to the solution. The acidified residues and the $BaSO_4$ precipitates were packed into folded tin cups with V_2O_5 for total sulfur and CAS sulfur isotope analysis, respectively. Uncertainties for carbon and sulfur isotope measurements determined by multiple analyses of standard materials during analytical sessions are better than 0.1% and 0.3‰, respectively.

Detrital zircon dating

For all aspects of zircon dating, we followed the procedures described in Martin *et al.* (2015). Zircon grains were isolated using conventional mineral separation techniques including rock pulverization by hand using a mortar and pestle, removal of silt and clay by hand panning in water, removal of magnetic grains using a Frantz magnetic barrier separator, and density separation using methylene iodide. Zircon grains were then poured onto double-sided tape and cast in an epoxy disk along with approximately 10 shards of the Sri Lanka zircon standard (564 ± 3 Ma) (Gehrels *et al.*, 2008). After hand polishing to expose the interiors of the grains, we produced backscattered electron and cathodoluminescence images using the JEOL JXA-8900R electron probe microanalyzer at the University of Maryland.

The cores of 49 and 175 zircon grains were dated from samples 09G-35.3 and 09G-37.9, respectively, by laser ablation-inductively coupled plasma-mass spectrometry in the Arizona LaserChron Center at the University of Arizona, taking care to avoid multiple cathodoluminescence zones, inclusions, and cracks. Ablation of the zircon was performed using a New Wave UP193HE Excimer laser and a spot diameter of 30 μm. The ablated zircon was carried in helium into the plasma source of a Nu Plasma HR multicollector mass spectrometer, and analyses followed the protocols described in Martin *et al.* (2015).

Corrections for interelement fractionation of Pb/U and common Pb, as well as other data reduction, were performed off-line using an Excel program developed at the Arizona LaserChron Center. We removed from further consideration analyses with: (i) high ^{204}Pb, (ii) greater than 5% error on the $^{206}Pb/^{207}Pb$ date, (iii) greater than 5% error on the $^{206}Pb/^{238}U$ date, (iv) greater than 25% normal discordance or 8% reverse discordance, (v) high U concentration, or (vi) high U/Th ratio. The remaining analyses were used in our interpretations (Table S1; Fig. 3). Isoplot was used to calculate weighted means and to produce concordia and probability density plots (Ludwig, 2008).

$^{206}Pb/^{238}U$ dates are usually more precise than $^{206}Pb/^{207}Pb$ dates for zircon younger than about 1.4 Ga, whereas the reverse is true for older grains. However, $^{206}Pb/^{207}Pb$ dates are only minimally affected by recent lead loss, so in most cases, they more closely indicate the time of crystallization for zircon older than about 1 Ga. Therefore, during interpretation, we used $^{206}Pb/^{238}U$ dates for grains younger than 1 Ga and $^{206}Pb/^{207}Pb$ dates for older zircon grains.

RESULTS

Detrital zircon from two closely spaced siltstone beds at 16.7 m (sample 09G-35.3) and 14.1 m (sample 09G-37.9) above the base of the Gaojiashan member yielded a youngest population of four U-Pb ages ranging from 543 to 550 Ma from sample 09G-37.9, with a weighted mean age of 548 ± 8 Ma (MSWD = 0.11) (Fig. 3, Table S1). This maximum depositional age based on detrital zircon measurements is consistent with the 551 Ma age estimate for the Miaohe Member beneath the Gaojiashan-equivalent Shibantan Member of the Dengying Formation based on U-Pb zircon age from the bedded ash layer (Amthor *et al.*, 2003; Condon *et al.*, 2005; Chen *et al.*, 2015). However, most of the detrital zircons in this study had ages between 750 and 850 Ma, with a scattering of solitary dates spanning from 1300 to 2700 Ma.

In total, 113 limestone and calcareous siltstone samples from the Gaojiashan Member were analyzed for elemental abundances and isotopic compositions (Figs 4–5; Tables S2–S4). Carbonate percentages in the samples are generally high (>90%), except in the lower member where limestones and siltstones are interbedded. The stratigraphic trend of $\delta^{13}C_{carb}$ variations reveals a positive carbon isotope excursion (up to +6‰) in the upper part of the Gaojiashan Member, coinciding with the fossil transition from *Conotubus* to *Cloudina*. Coupled with the positive $\delta^{13}C_{carb}$ event, $\delta^{13}C_{org}$ data reveal a negative excursion (down to –30‰); calculated carbon isotope fractionations ($\Delta\delta^{13}C_{carb\text{-}org}$) show peak values up to +36‰ in this interval. Pyrite S isotope ($\delta^{34}S_{pyrite}$) values measured from bulk acidified residues (assuming pyrite S ≫ organic S) show a wide range from −30‰ to +30‰ in the Gaojiashan Member, with more negative values in the lower half of the section, and more positive values in the upper half. On the contrary, sulfur isotope compositions of carbonate-associated sulfate ($\delta^{34}S_{CAS}$) remain

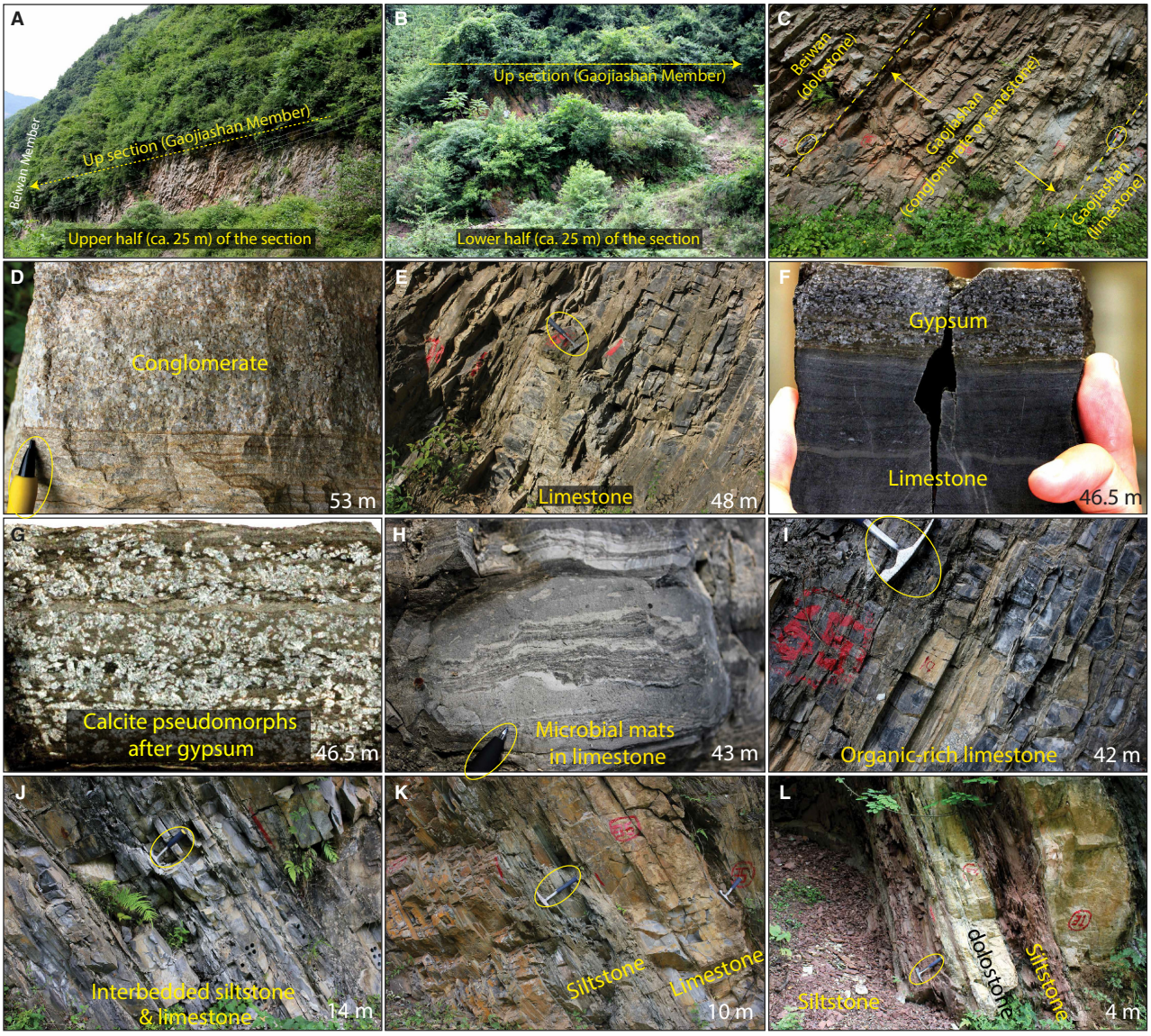

Fig. 2 Field photographs of the Gaojiashan Member. Hammers or pencils for scale and meterages above the base of the unit. (A, B) An overview of the upper and lower section (each ca. 25 m in thickness). (C) Boundary between the Beiwan and Gaojiashan members. (D) Conglomerate in the uppermost interval. (E) Bedded limestone at 48 m. (F, G) Gypsum pseudomorphs at 46.5 m where crystals have been dissolved and replaced by calcite. (H, I) Organic-rich limestones with abundant microbial mats corresponding to the peak of the carbon isotope excursion at ca. 43 m. (J) Interbedded siltstone and limestone at 14 m. (K, L) Siltstones in the lower Gaojiashan Member.

generally invariant around ca. +40‰ throughout the Gaojiashan Member. Both total sulfur (TS) and total organic carbon (TOC) are relatively low through most of the succession, but are elevated in the cloudinid interval. Mg/Ca ratios show the dominance of limestone in the Gaojiashan Member, with higher Mg/Ca, Mn/Sr, and Rb/Sr ratios found only in dolostones interbedded with siltstones in the lower Gaojiashan Member. Sr/Ca ratios reveal a positive excursion in the upper section, mimicking the $\delta^{13}C_{carb}$ anomaly, whereas Ce/Ce* ratios through the section remain constant at values near to 0.5, with the exception of two samples at the top of the Gaojiashan Member with higher values.

DISCUSSION

Diagenesis

Confidence in our ability to interpret environmental changes associated with the paleontological transitions in the Gaojiashan requires that we evaluate the degree of alteration of the limestone samples. Based on the low

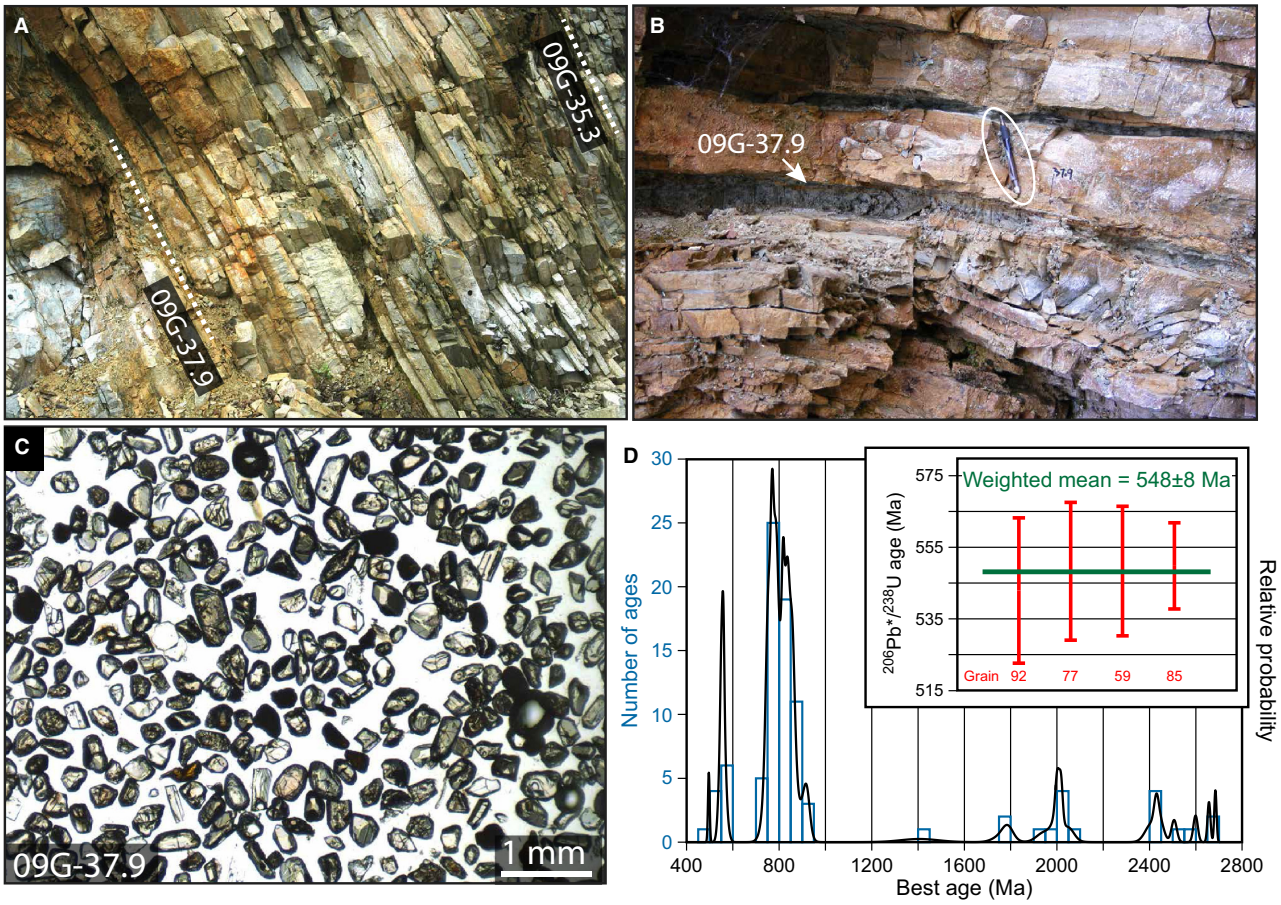

Fig. 3 (A) Field photograph showing the position of the two detrital zircon samples (09G-35.3, 09G-37.9) in the lower Gaojiashan Member. The view is about 3 m wide. (B) Close view of bed 09G-37.9. (C) Separated and mounted detrital zircon from sample 09G-37.9. (D) Histogram and relative probability plot for detrital zircon ages from sample 09G-37.9. Best age is $^{206}Pb/^{238}U$ date for grains younger than 1 Ga and $^{206}Pb/^{207}Pb$ date for older zircon. Histogram bars represent 50 Ma intervals. Inset: $^{206}Pb/^{238}U$ ages for the four youngest analyses with uncertainties that overlap at the 1-sigma level. The weighted mean of these four ages is 548 ± 8 Ma (MSWD = 0.11) from which we interpret a maximum possible depositional age of 560 Ma.

Mn/Sr and Rb/Sr, and the smooth temporal trends in other geochemical indicators defined by high-resolution sampling, the limestones appear to be especially well preserved (Fig. 4). However, insofar as carbonates are susceptible to isotopic exchange with meteoric or hydrothermal fluids after burial, stable isotope compositions of carbonate phases might reflect diagenetic overprints over depositional signatures. For example, the lithification of marine carbonates associated with the flushing of meteoric fluids could cause coupled depletions in both ^{13}C and ^{18}O, assuming the alkalinity was sourced from soil respiration (Knauth & Kennedy, 2009). Isotopic coupling in carbonates might also result from burial diagenesis (Derry, 2010; Bristow *et al.*, 2011) assuming hot fluid temperatures and alkalinity formed through anaerobic processes. In either case, the carbonates would be predictably recrystallized or contain appreciable amounts of neomorphic calcite. These petrographic features are not observed in the fine-grained Gaojiashan limestones, which reveal a significant positive $\delta^{13}C_{carb}$ excursion, whereas $\delta^{18}O_{carb}$ values remain steady. A cross-plot of the carbon and oxygen isotope abundances in these samples reveals no positive correlation (Fig. 5, lower panel). Insofar as oxygen isotopes would be more likely to be altered during water-rock interactions (Jacobsen & Kaufman, 1999), the $\delta^{13}C_{carb}$ excursion recorded in the Gaojiashan Member is likely to reflect true secular changes in seawater composition.

The degree of carbonate preservation may also be evaluated through the analyses of CAS abundances and sulfur isotope compositions. Published studies have shown that CAS in marine carbonates may be affected by secondary processes related to pyrite oxidation (Marenco *et al.*, 2008), which could occur in the outcrop or in the laboratory, or the addition of secondary atmospheric sulfate (SAS) to carbonates exposed in desert environments (Peng *et al.*, 2014). On the other hand, CAS studies of modern carbonate sediments where there was active pore-water sulfate reduction indicate minimal alteration of bulk carbonate

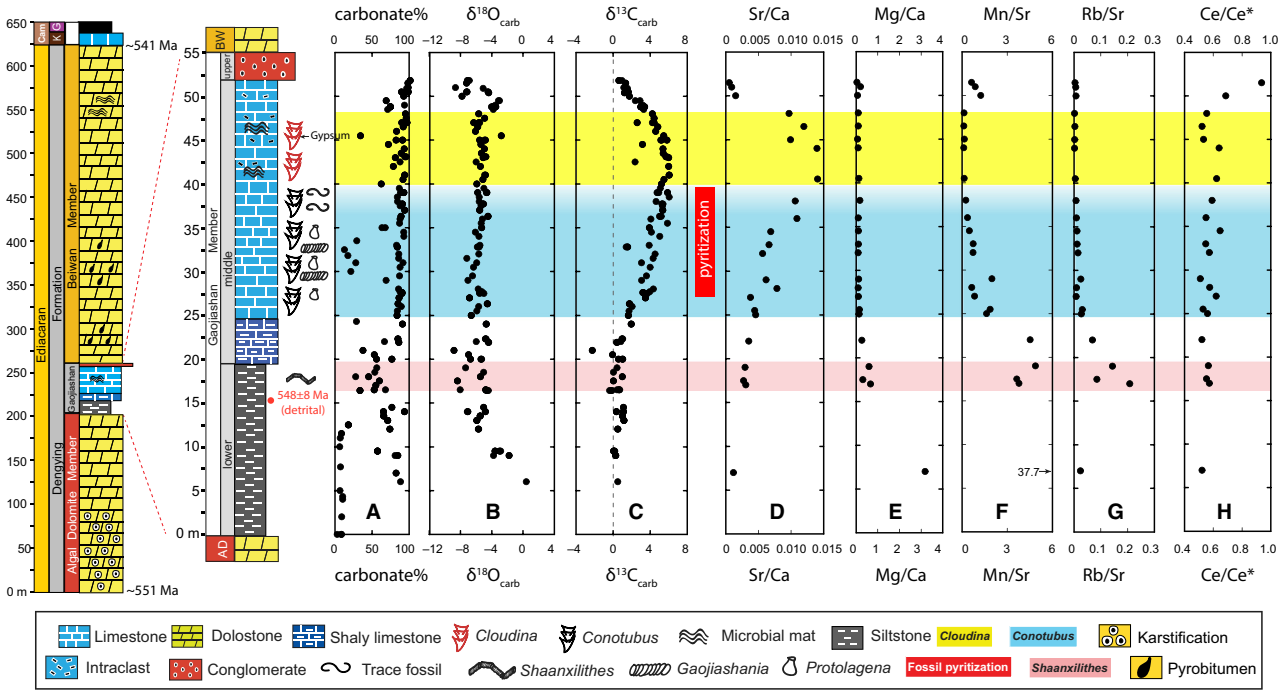

Fig. 4 Integrated litho-, bio-, and chemo-stratigraphy of the Gaojiashan Member, including fossil occurrences of *Conotubus* and *Cloudina*, as well as geochemical profiles of carbonate content (wt. %), carbonate carbon ($\delta^{13}C_{carb}$, ‰ V-PDB) and oxygen ($\delta^{18}O_{carb}$, ‰ V-PDB) isotopes, Sr/Ca, Mg/Ca, Rb/Sr, Mn/Sr, and Ce anomaly (Ce/Ce*) calculated using the formula $Ce/Ce^* = Ce_{PAAS}/([Pr]^2_{PAAS}/[Nd]_{PAAS})$ (Ling *et al.*, 2013). K = Kuanchuanpu, G = Guojiaba, Cam = Cambrian, BW = Beiwan, AD = Algal Dolomite.

sulfur isotope compositions (Lyons *et al.*, 2004). While Gaojiashan CAS abundances are generally low (ranging from near 0 to 150 ppm), their $\delta^{34}S_{CAS}$ values are invariant at ca. +40‰ throughout the succession (Fig. 5F,G), suggesting excellent preservation of primary signals (Gill *et al.*, 2008). The sulfur isotope invariance, which is notably consistent with $\delta^{34}S_{sulfate}$ analyses of bedded anhydrites (ca. +40‰) in equivalent terminal Ediacaran strata from Oman (Fike & Grotzinger, 2008), supports the view that the Gaojiashan carbonates are exceptionally well preserved and likely reflective of global seawater conditions.

To further evaluate diagenesis in the Gaojiashan Member samples, we compared abundances of TOC and pyrite against each other, as well as with their carbon and sulfur isotope compositions, respectively. In neither case do we see a systematic relationship (Fig. 5 lower panel), although the two samples with the highest TOC do have the lowest $\delta^{13}C$ signatures. TOC might change by either microbial (Borowski *et al.*, 1996, 2013; Jørgensen *et al.*, 2004; Ries *et al.*, 2009) or thermochemical (Cai *et al.*, 2001, 2003, 2004) sulfate reduction after deposition, which could result in progressive ^{34}S-enrichment of product sulfide preserved as pyrite. However, the sedimentary rocks have not been buried deeply enough to drive the thermal reactions. Furthermore, we find no systematic relationship in TOC–TS or TOC–$\delta^{34}S$ cross-plots, suggesting that these secondary processes did not significantly impact the Gaojiashan samples.

Redox constraints for the Gaojiashan Member

Multiple lines of evidence suggest that the paleontological transition in the middle Gaojiashan Member is accompanied by strong ocean stratification (Figs 5 and 6). Support for this interpretation comes from the negative excursion in the ^{13}C abundance of TOC – which mirrors the positive $\delta^{13}C_{carb}$ excursion – resulting in the greatest magnitude of $\Delta\delta^{13}C$ values in the *Cloudina* interval (Fig. 5A–C). In light of the abundance of microbial fabrics in both the Gaojiashan Member (Cai *et al.*, 2010) and the Nama Group (Bouougri & Porada, 2007), these decoupled chemostratigraphic carbon isotope trends could plausibly have resulted from organic matter derived from benthic microbial mats where anaerobic chemoautotrophs utilized locally recycled ^{13}C-depleted DIC to form biomass with lower $\delta^{13}C_{org}$ values (Des Marais, 1990; Hayes, 1993; Falkowski *et al.*, 2008; Houghton *et al.*, 2014). Alternatively, there may have been an enhanced flux of organic matter derived from anoxygenic photoautotrophs such as green and purple sulfur bacteria that utilize H_2S as a source of electrons during photosynthesis (Johnston *et al.*, 2009). These photoautotrophs typically exist along redox

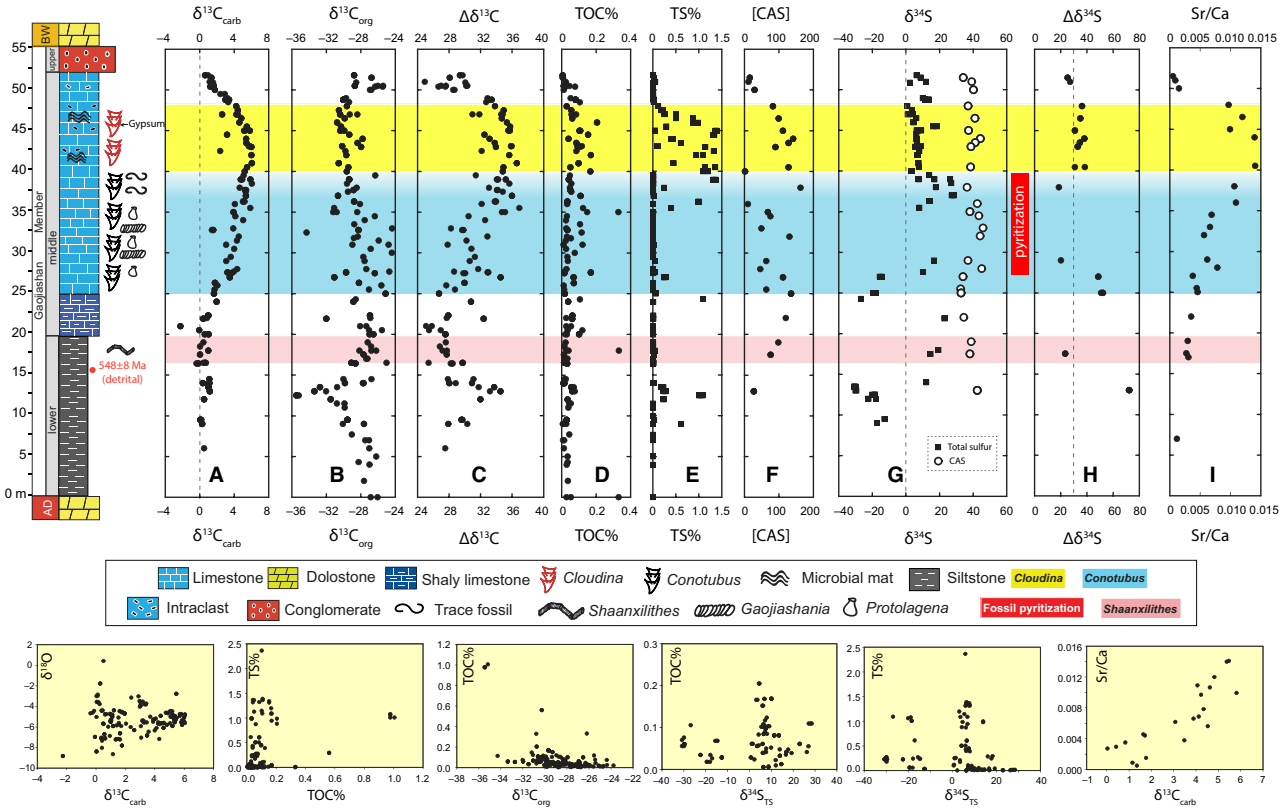

Fig. 5 Integrated litho-, bio-, and chemo-stratigraphy of the Gaojiashan Member, including fossil occurrences of *Conotubus* and *Cloudina*, as well as geochemical profiles of carbonate carbon ($\delta^{13}C_{carb}$, ‰ V-PDB) and organic carbon ($\delta^{13}C_{org}$, ‰ V-PDB) isotopes, carbon isotope fractionations ($\Delta\delta^{13}C_{carb\text{-}org}$), pyrite sulfur ($\delta^{34}S_{TS}$, ‰ V-CDT) and CAS sulfur ($\delta^{13}C_{CAS}$, ‰ V-CDT) isotopes, sulfur isotope fracionations ($\Delta\delta^{34}S_{CAS\text{-}pyrite}$), total organic carbon content (TOC), total sulfur content (TS, dominated by pyrite with trace amount of organic S), carbonate-associated sulfate concentration ([CAS] in ppm). The cross-plots below the main figure show the relationships of $\delta^{13}C_{carb}$–$\delta^{18}O_{carb}$, TOC–TS, $\delta^{13}C_{org}$–TOC, $\delta^{34}S_{TS}$–TOC, $\delta^{34}S_{TS}$–TS, $\delta^{13}C_{carb}$–Sr/Ca. BW = Beiwan, AD = Algal Dolomite.

chemoclines and utilize respired CO_2, which is typically depleted in ^{13}C relative to its atmospheric equivalent (e.g., Brocks *et al.*, 2005). In either case, the spread of anoxic/euxinic conditions across the platform would have promoted organic matter burial (Hayes *et al.*, 1983) and the positive $\delta^{13}C_{carb}$ excursion. High abundances of organic S compounds, indicative of euxinic conditions, are also revealed by biomarker studies of the Gaojiashan-equivalent Shibantan Member (Duda *et al.*, 2014). Further evidence for the spread of anoxia associated with the decoupled $\delta^{13}C$ excursions is found in the profoundly negative $\delta^{238}U$ signatures of Gaojiashan limestones (Zhang *et al.*, 2015), and our sulfur isotope measurements.

Chemostratigraphic analyses of the Gaojiashan Member reveal a profound rise in $\delta^{34}S_{pyrite}$ values from as low as −30‰ in the lower half of the member to peak values near +30‰ between 35 and 40 m before falling rapidly to values averaging around +10‰ in the *Cloudina*-bearing beds (Fig. 5G). In contrast, the $\delta^{34}S$ of CAS remain steady at values of ca. +40‰ throughout the Gaojiashan Member. The calculated sulfur isotope contrasts ($\Delta\delta^{34}S$) range widely in the lower half of the succession, with a maximal value of 72‰, but in the upper half $\Delta\delta^{34}S$ is relatively constant at ca. 30–35‰ (Fig. 5H). Interpreting the environmental significance of these remarkable stratigraphic variations requires the recognition that the $\delta^{34}S_{CAS}$ and $\delta^{34}S_{pyrite}$ signatures are inherited from different parts of the depositional basin. Sulfate incorporation into primary carbonate sediments would occur within the water column, whereas pyrite would form either in euxinic bottom waters or within sediments. Considering this spatial separation, local sulfate availability could dictate the $\delta^{34}S$ isotopic difference between CAS and pyrite, particularly if pyrite is formed in non-bioturbated and microbially sealed sediments where the water–sediment interface represents a significant diffusion barrier (Bottjer *et al.*, 2000; Bouougri & Porada, 2007; Fike *et al.*, 2008, 2009). While such a scenario might apply to discrete intervals within the Gaojiashan—including the *Shaanxilithes* and *Conotubus* zones (Fig. 5H)—other parts of the succession have measured $\Delta\delta^{34}S$ differences that are significantly larger. Furthermore, the constancy of the $\delta^{34}S_{CAS}$ values through the Gaojiashan suggests that the perturbation in the terminal Ediacaran sulfur cycle did not involve changes in the marine

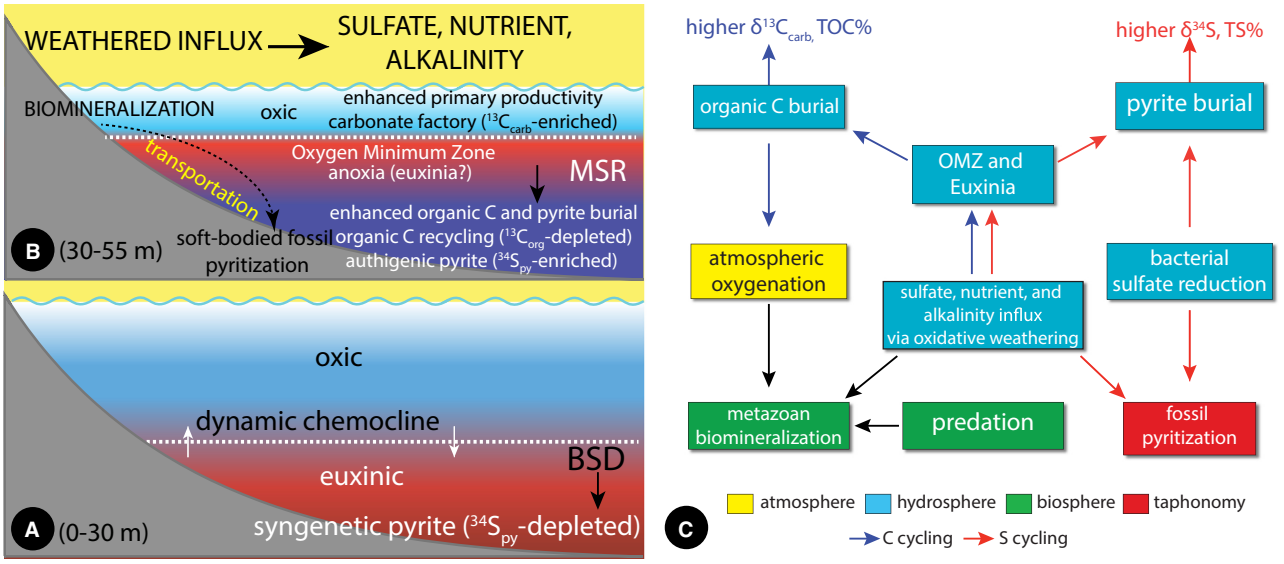

Fig. 6 Conceptual weathering and biogeochemical model for the Gaojiashan Member. (A) During Stage 1, the basin was stratified with oxic surface water above euxinic deepwater. Bacterial S disproportionation (BSD) may be an important contributor to the sulfur cycle. (B) During Stage 2, the basin was strongly influenced by the spread of an oxygen minimum zone (OMZ) beneath oxic surface waters. This likely occurred as a result of sea level regression and enhanced continental weathering, which resulted in a larger sulfate pool in the ocean, elevated ocean alkalinity, and microbial sulfate reduction (MSR) as the dominant pathway for microbial sulfur cycling. (C) Biogeochemical feedback that links the carbon and sulfur cycles to atmospheric oxygenation, animal evolution, and fossil preservation.

sulfate isotopic composition. Thus, the ~60‰ shift in $\delta^{34}S$ of pyrite from the lower to the upper Gaojiashan Member may require a change in biologically induced fractionations involving both the reductive and oxidative paths of the sulfur cycle (i.e., bacterial S disproportionation, or BSD) (Canfield & Thamdrup, 1994), or microbial sulfate reduction (MSR) with very low sulfate reduction rates (SRR) (Canfield *et al.*, 2010; Leavitt *et al.*, 2013; Wu & Farquhar, 2013; Wing & Halevy, 2014).

In the case of BSD, sulfur is recycled via both reductive and oxidative pathways. On the reductive side, the magnitude of kinetic sulfur isotope fractionation (ε_{SR}) has been observed to correlate directly with extracellular sulfate concentrations. Experiments from pure cultures of sulfate reducers indicate maximal fractionation of 66‰ at sulfate concentrations similar to modern seawater at 28 mM (Sim *et al.*, 2011), while ε_{SR} may be suppressed at very low sulfate abundances (<200 μM) (Habicht *et al.*, 2002). On the oxidative side, the sulfide produced through MSR is typically re-oxidized to elemental sulfur, which is subsequently disproportionated to sulfate and sulfide, by coupling with the reduction of O_2, NO_3^-, or iron and manganese compounds (Canfield & Thamdrup, 1994). Disproportionation reactions thus can significantly augment the fractionations induced during MSR, resulting in isotopic contrasts between reactant sulfate and product sulfide of >70‰ (Fig. 5H).

Alternatively, very low rates of MSR may also lead to large fractionations. Recent studies of lacustrine euxinic systems indicate that >70‰ fractionations are achievable by both isolated and natural populations of sulfate reducers (Canfield *et al.*, 2010; Gomes & Hurtgen, 2015). Furthermore, environmentally controlled experiments suggest that MSR-related fractionation could be strain specific (Bradley *et al.*, 2016), or related to SRR that are dependent on the availability of organic substrates as electron donors (Canfield *et al.*, 2010; Leavitt *et al.*, 2013; Leavitt, 2014; Wing & Halevy, 2014; Gomes & Hurtgen, 2015). In this case, the magnitude of fractionation is inversely correlated with the rate of sulfate reduction (e.g., Xiao *et al.*, 2010). With these constraints in mind, the $\Delta\delta^{34}S$ >70‰ in the lower interval of the Gaojiashan may reflect BSD coupled with MSR, or result solely from MSR with very low SRR. The former scenario is consistent with sulfide oxidation occurring along a chemocline above euxinic deep waters (Fig. 6A), which is our preferred interpretation for this marginal marine basin.

Based on systematic studies of modern environments and Phanerozoic shales (Berner & Raiswell, 1983, 1984), very low C/S ratios might indicate euxinic marine conditions. Although the C/S proxy is not well calibrated for carbonates, the preponderance of Gaojiashan limestones with values <1 (Fig. 5 lower panel) suggests the possibility of euxinic conditions in the depositional basin. This view is consistent with the high Ce/Ce* values in the upper Gaojiashan samples (Fig. 4H), although carbonates have notoriously low REE abundances and should thus be interpreted with caution.

Global indicators of dynamic redox conditions

Chemostratigraphic comparison of terminal Ediacaran successions in South China, Oman, and Namibia reveals both similarities and differences, suggesting local overprint of global signals in some basins (e.g., Loyd *et al.*, 2013; Wood *et al.*, 2015) (Fig. 7). Global conditions appear to be reflected in the similarity in the magnitude and direction of isotope trends in South China and Oman. For example, in the uppermost Buah Formation of Oman, paired CAS-pyrite measurements reveal large magnitude sulfur isotope fractionations (with maximal $\Delta\delta^{34}S \sim 50‰$) prior to the first occurrence of *Cloudina* (Conway Morris *et al.*, 1990), just as we document for the lower Gaojiashan Member. The large fractionation seen in two basins suggests the dominance of sulfur disproportionation reactions (Fike *et al.*, 2006; Fike & Grotzinger, 2008), which is supported by a recent multiple sulfur isotope study indicating enhanced sulfide re-oxidation in the uppermost Buah (Wu *et al.*, 2015). In this interval, disproportionation reactions likely dominated over MSR insofar as the latter would be discouraged if there was active photoautotrophic sulfide oxidation (Fig. 6A) (Habicht & Canfield, 2001). Stratigraphically higher in the Ara Formation where *Cloudina* occurs in carbonates interbedded with evaporites, the $\delta^{34}S$ compositions of pyrite and CAS are notably invariant with a smaller magnitude of fractionation (ca. 30‰) (Fike & Grotzinger, 2008), again exactly matching our observations from the upper Gaojiashan. The ^{34}S enrichments in pyrite and the smaller sulfur isotope differences between reduced and oxidized phases are best explained by high rate of MSR, which we view as the dominant sulfur metabolism associated with the spread of anoxic bottom waters (Fig. 6B,C). In sum, the correlated observations from South China and Oman indicate a global environmental control on biological sulfur fractionations.

To the contrary, chemostratigraphic data from *Cloudina*-bearing strata of the Nama Group in southern Namibia provide a completely different pattern of ^{34}S enrichments and fractionation. In this case, strongly positive $\delta^{34}S_{pyrite}$ values are most-often paired with anomalously low and scattered $\delta^{34}S_{CAS}$ values, resulting in inversely fractionated $\Delta\delta^{34}S$ values (Ries *et al.*, 2009). Stratigraphically coherent CAS results are only seen in the Omkyk Member where there is a positive $\delta^{34}S_{CAS}$ shift from ca. +10 up to +40‰, which is similar to the trend encompassing the transition to the *Cloudina*-bearing beds in Oman and South China (Fig. 7), and in the uppermost Spitzkop Member below the Ediacaran–Cambrian boundary. In this case, however, the CAS sulfur isotope compositions are depleted in ^{34}S by ~20‰ relative to equivalent upper Ara strata in Oman. Based on our experience with quantitative preparation techniques, it would appear that the Namibian CAS samples were not adequately leached of non-CAS components. In contrast to our extensive efforts to remove the non-carbonate fraction (see Methods), Ries *et al.* (2009) leached the CAS powders with Milli-Q water only once, and this is unlikely to have quantitatively removed sulfate on mineral surfaces

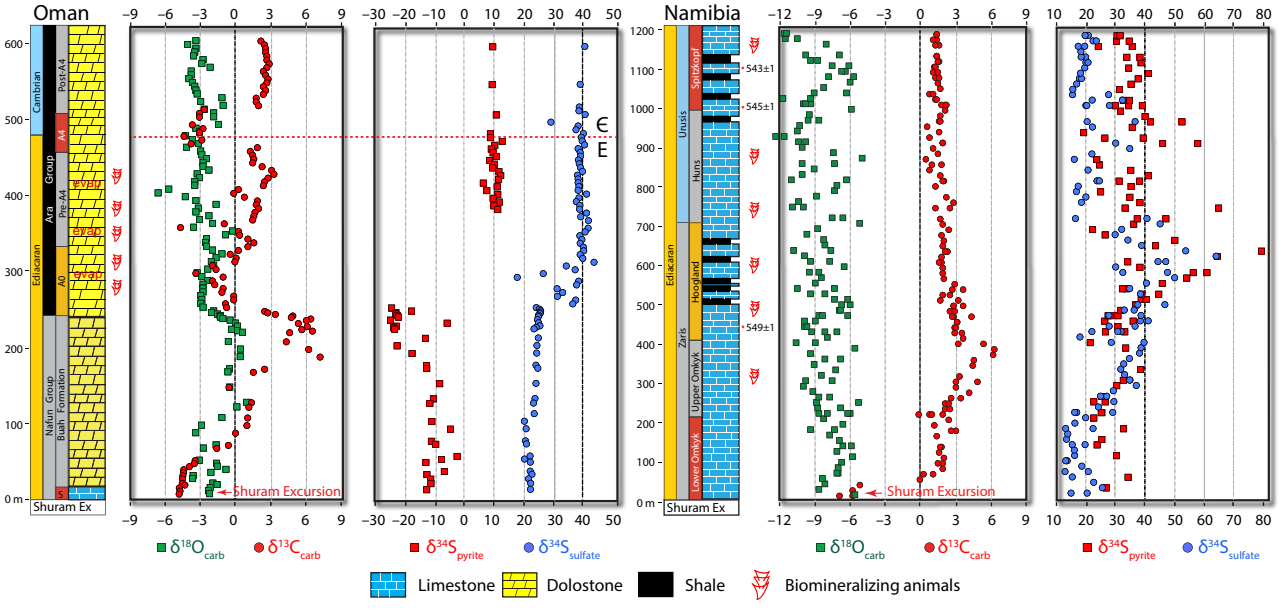

Fig. 7 Integrated carbon and sulfur isotopic profiles from late Ediacaran strata in Oman (Fike & Grotzinger, 2008) and Namibia (Ries *et al.*, 2009). The remarkable difference in sulfur isotope trends between Oman and Namibia may result from effects of local conditions (e.g., different organic carbon flux, sulfate concentration) on microbial sulfate reduction rate and sulfur isotope fractionations, but may also reflect analytical issues (see text).

formed through pyrite oxidation (Marenco *et al.*, 2008) or SAS (Peng *et al.*, 2014). The presence of these contaminants would cause $\delta^{34}S_{CAS}$ values to be more negative and hence would not reflect depositional signatures (Wotte *et al.*, 2012). In our view, the inversely fractionated sulfur isotopes from this succession should be interpreted with caution, although they do highlight the potential redox differences between equivalent terminal Ediacaran basins.

In addition, there are notable contrasts in carbon isotope anomalies among the terminal Ediacaran successions in South China, Oman, and Namibia. Chemostratigraphic data from the Dengying Formation suggest the possibility of three separate positive excursions (Fig. 1), with their different stratigraphic thicknesses likely associated with varying sediment accumulation rates. In contrast, there is significant $\delta^{13}C_{carb}$ variability in the evaporite-rich succession from Oman (Fike & Grotzinger, 2008; Wu *et al.*, 2015), including negative anomalies within the cloudinid interval interspersed with at least two positive excursions (Fig. 7). In Namibia, there is only one post-Shuram positive $\delta^{13}C_{carb}$ excursion followed by a long plateau of moderately positive (ca. +1 to +3‰) values leading up to the Ediacaran–Cambrian boundary (Fig. 7) (Ries *et al.*, 2009). Other terminal Ediacaran successions, including those in northern India, also reveal significant differences in carbon isotope stratigraphic profiles (Kaufman *et al.*, 2006). Taken together, the interbasinal variations in carbon and sulfur isotope compositions likely reflect redox differences in the depositional environments of the various basins. If correct, the Ediacaran experiment in animal life must have been spread across a dynamic environmental landscape, which may help to explain the distribution of geographically unique assemblages (Narbonne *et al.*, 2014).

Enhanced alkalinity in the terminal Ediacaran ocean

Compared with carbonates in the underlying Doushantuo Formation (e.g., McFadden *et al.*, 2008), the generally lower TOC contents of the Gaojiashan limestones are notable, and may reflect either depositional or early diagenetic processes. For example, pervasive water column or sediment recycling of organic matter may have decreased original organic carbon contents in sediments. In addition, the anaerobic conversion of simple organic compounds to alkalinity could have resulted in the formation of ubiquitous authigenic carbonates (Higgins *et al.*, 2009; Schrag *et al.*, 2013). Driven by iron or sulfate reduction of available organic substrates, the addition of authigenic carbonate to the sediments would, however, have resulted in a negative (rather than a positive) carbon isotope excursion. Alternatively, the generally lower TOC values may reflect significant dilution by abundant carbonate formed from highly alkaline seawater. In this case, the source of the alkalinity was more likely to be from terrestrial weathering, as indicated by the significant rise in $^{87}Sr/^{86}Sr$ in the terminal Ediacaran Period (Kaufman *et al.*, 1993, 1997; Halverson *et al.*, 2007; Sawaki *et al.*, 2010; Cui *et al.*, 2015). The abundance and carbon isotopic composition of river-derived alkalinity in the Ediacaran Period was likely to be highly variable, depending on the differential weathering of bedrock lithologies (e.g., carbonates vs. silicates). In the absence of land plants or extensive microbial surfaces, terrestrial sources of alkalinity need not have been significantly depleted in ^{13}C. Elevated seawater alkalinity at this time is consistent with the presence of aragonite crystal fans preserved in the time-equivalent Nama Group in Namibia (Grotzinger, 2000; Grotzinger *et al.*, 2005; Hall *et al.*, 2013), which records a singular Ediacaran positive $\delta^{13}C_{carb}$ excursion (Kaufman *et al.*, 1991; Saylor *et al.*, 1998). Overall high alkalinity is also consistent with the dominance of carbonate in terminal Ediacaran successions worldwide and may explain the extremely high accumulation rate estimated for the Dengying (i.e., >650 m in ~10 million years), as compared with the underlying Doushatuo (i.e., <200 m in ~84 million years) (Fig. 1).

Enhanced terminal Ediacaran alkalinity may also be interpreted from our elemental results from the Gaojiashan, as well as interbasinal and intrabasinal equivalents. In particular, the [Sr] and Sr/Ca data measured from the Gaojiashan limestones reveal positive excursions in step with the positive $\delta^{13}C_{carb}$ anomaly (Fig. 8). A similar [Sr] excursion coincident with peak $\delta^{13}C$ compositions of carbonates is noted in the Gaojiashan-equivalent Shibantan Member in the Yangtze Gorges area (Sawaki *et al.*, 2010). A rise in [Sr] is also noted in the broadly equivalent Nama Group in southern Namibia (Ries *et al.*, 2009) although this geochemical anomaly postdates the first appearance of *Cloudina* and the singular positive $\delta^{13}C$ excursion in the thick sedimentary succession. The apparent [Sr] rise in Namibia is potentially complicated by the addition of Sr from siliciclastics admixed with the carbonates due to the use of aqua regia (Ries *et al.* 2009), which would attack both carbonate and siliciclastic components during dissolution. Nonetheless, all sections show positive [Sr] excursion in *Cloudina*-bearing intervals. For the Gaojiashan, the invariantly low Mg/Ca values of samples suggest that dolomitization played no role in the elemental excursion (Fig. 4).

Given that the dominant source of Sr in the ocean is from the chemical weathering of the continental crust (Shields, 2007; McArthur *et al.*, 2012), including both silicates and carbonates, enhanced [Sr] and Sr/Ca values supports the view that terrestrial weathering and the delivery of alkalinity through riverine inputs buffered shallow ocean basins to variable degrees in the terminal Ediacaran Period. The weathering of Ca silicate minerals can be simply represented by the overall reaction (Berner, 2004): $CO_2 + CaSiO_3 \rightarrow CaCO_3 + SiO_2$, which over geological

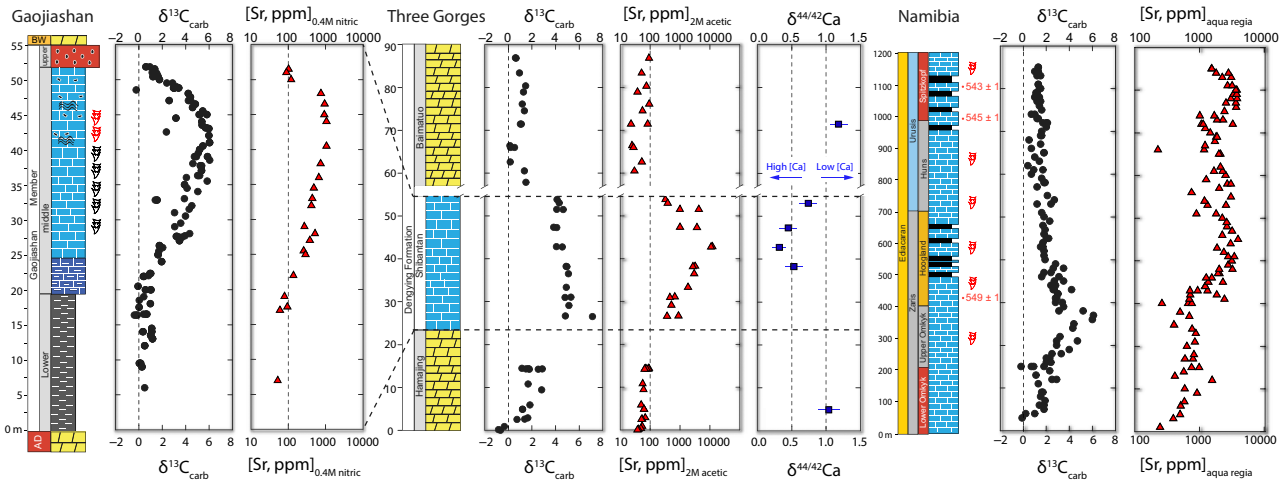

Fig. 8 Integrated litho-, bio-, and chemo-stratigraphy of the terminal Ediacaran Gaojiashan Member in the study area, Yangtze Gorges area, and Namibia, including geochemical profiles of carbonate carbon isotopes ($\delta^{13}C_{carb}$, ‰ V-PDB), strontium concentration ([Sr] in ppm, plotted in log scale), and $\delta^{44/42}Ca$ (‰). Ca isotope ratios are given relative to NIST SRM 915a. Data for the section in Yangtze Gorges area are from Sawaki *et al.* (2010, 2014). Data for the section in Namibia are from Ries *et al.* (2009). Note that the Sr concentrations are measured using different acids in different studies. The negative $\delta^{44}Ca$ excursion in the Gaojiashan-equivalent Shibantan Member has been interpreted to reflect high Ca concentration in terminal Ediacaran seawater (Sawaki *et al.*, 2014).

time scales sequesters atmospheric CO_2 into carbonate minerals by liberating Ca^{2+} and HCO_3^- ions that are then carried to seawater by rivers. While terrestrial carbonate weathering is not a geological sink for atmospheric CO_2, the resultant flux of alkalinity does effect overall carbonate saturation state (e.g., Kump *et al.*, 1999; Hoffman & Schrag, 2002; Higgins & Schrag, 2003).

Associated with higher alkalinity and higher carbonate saturation, it should be noted that Sr/Ca may also be controlled by precipitation rate. For biogenic carbonates (e.g., coccoliths), the ratio of Sr to Ca has been widely used as a productivity proxy (e.g., Stoll & Schrag, 2001; Stoll & Bains, 2003) insofar as there is a strong link between Sr/Ca, export production, and calcification rate (Stoll & Schrag, 2001). Similarly, laboratory experiments reveal that rapid precipitation rates induce greater Sr partitioning into abiotic calcite (Lorens, 1981; Tesoriero & Pankow, 1996; Tang *et al.*, 2008; DePaolo, 2011). Thus, the precipitation rate of carbonate in either *Cloudina* or in inorganic micrite may have additionally influenced the Sr/Ca ratios of the Gaojiashan limestones.

Variable partitioning of strontium by aragonite and calcite relative to seawater may also have resulted in the observed variations of Sr/Ca in the Gaojiashan samples. Strontium has a crystal ionic radius larger than that of Ca^{2+} and thus prefers the more open octahedral crystal structure of aragonite over the smaller hexagonal structure of calcite (Wray & Daniels, 1957; Lorens, 1981). Thus, on the one hand, the enhancement in [Sr] in the Gaojiashan limestones and their equivalents might reflect a secular change from calcite to aragonite-dominated seas (e.g., Stanley & Hardie, 1998), although the short stratigraphic interval represented by the Gaojiashan Member would seem to preclude this possibility. On the other, the [Sr] excursion might result from postdepositional diagenesis, through which Sr was preferentially flushed from specific horizons in the Gaojiashan Member during neomorphic aragonite-to-calcite transformations (Katz *et al.*, 1972). However, given the excellent petrographic and oxygen isotopic preservation of the samples, the absence of dolomitization, and smooth carbon and sulfur isotope trends, we attribute the elevated Sr/Ca ratios in the *Cloudina* interval to (i) elevated Sr flux from the continents to contemporaneous seawater and/or (ii) enhanced precipitation rate in a carbonate over saturated ocean.

Emerging support for weathering-induced high alkalinity in terminal Ediacaran seawater may come from Ca isotope ($\delta^{44}Ca$) measurements of the Gaojiashan-equivalent Shibantan Member. In this unit, a sharp negative $\delta^{44}Ca$ excursion (down to 0.3‰) has been interpreted to reflect anomalously high seawater Ca concentrations. The Ca isotope system has been used to make inferences regarding the seawater Ca cycle in deep time (DePaolo, 2004; Nielsen *et al.*, 2011), with a special emphasis on perturbations of $\delta^{44}Ca$ during chemical weathering events. Enhanced chemical weathering in the Cenozoic (between 40 and 10 Ma), for example, has been interpreted based on the presence of negative $\delta^{44}Ca$ excursions (De La Rocha & DePaolo, 2000; DePaolo, 2004). Similarly, a Cretaceous negative $\delta^{44}Ca$ excursion believed to be related to enhanced weathering (Blättler *et al.*, 2011) coincides with a positive $\delta^{13}C$ anomaly and an Oceanic Anoxic Event, all of which match our observations of the Gaojiashan.

In concert, the sedimentological and geochemical observations of *Cloudina*-bearing strata in South China and elsewhere suggest that the terminal Ediacaran ocean was highly alkaline. If correct, high concentrations of Ca and alkalinity well may have enabled the earliest example of calcareous biomineralization by animals.

Environmental context of pyritization and biomineralization

Based on our chemostratigraphic observations of the Gaojiashan Member, the first appearance of *Cloudina* coincided with the development of anoxic and episodically euxinic conditions across the shelf environment. It is likely, however, that this first biomineralized metazoan lived in the oxidized shallower water column and was swept into deeper anoxic settings by storm events (Cai *et al.*, 2010) (Fig. 5B). In contrast, our geochemical results suggest that *Conotubus* and other soft-bodied Ediacara biotas thrived at a time of more generally oxidizing conditions within the water column prior to the peak of the $\delta^{13}C$ excursion. In the equivalent Shibantan Member in the Yangtze Gorges region, the soft-bodied organisms are preserved in subtidal environments and are closely associated with abundant bilaterian burrows, suggesting moderate levels of bioturbation (Chen *et al.*, 2013, 2014; Meyer *et al.*, 2014). It is notable that *Conotubus* and many Ediacara remains, as well as the microbial surfaces, were preserved in these environments through pyritization (Gehling, 1999; Schiffbauer *et al.*, 2014). In the 'death mask' model, pyritization of a decomposing metazoan would stabilize its surface and allow the external form of the organism to be imprinted with exquisite detail; in the case of the Gaojiashan Member, similar pyritization process may have also molded *Conotubus* tubes from inside. Based on *in situ* SIMS $\delta^{34}S$ analyses, it has been proposed that pyritization of *Conotubus* was fueled by the degradation of labile organic tissues through MSR (Schiffbauer *et al.*, 2014) near the sediment–water interface. Consistent with pyritization as a widespread fossilization pathway, many soft-bodied fossils and associated microbial surfaces in the Gaojiashan and Shibantan exposures are coated with iron oxides and jarosite (an iron-bearing sulfate mineral) that are the oxidative weathering products of early diagenetic pyrite (Hall *et al.*, 2013).

The balance between the ecological pressures and physiological responses that resulted in the biomineralization of *Cloudina* is nicely viewed from the Gaojiashan Member and its equivalents in South China. On the one hand, Hua *et al.* (2003) highlighted the large number of drill holes on *Cloudina* shells in the Dengying Formation and hypothesized that predation tipped the balance toward calcification as a means of protection. On the other hand, our results emphasize clear temporal changes in seawater chemistry that are associated with this evolutionary milestone. We interpret the geochemical trends to reflect enhanced terminal Ediacaran chemical weathering that introduced nutrients, which drove primary productivity, the spread of anoxia, and higher rates of organic carbon burial. Chemical weathering would also have delivered alkalinity and cations including calcium to seawater, promoting rapid carbonate accumulation in shallow marine settings. In addition, sulfate delivery would have further stimulated MSR, which would provide an additional source of seawater alkalinity depending on the extent of water column anoxia. Biomineralization could then have been a means to remove excess calcium from the newly developed circulatory systems of evolving metazoans (Simkiss, 1977) in the context of higher overall seawater alkalinity in the terminal Ediacaran Period (Grotzinger *et al.*, 2005).

Studies of Phanerozoic biomineralization further highlight the effect of seawater chemistry on calcification. Although the secretion of biominerals often occurs in internal environments isolated from seawater (Weiner & Dove, 2003), seawater chemistry could indirectly determine skeletal mineralogy by affecting the physiological costs of biomineralization (Knoll, 2003a), thus resulting in distinct patterns of skeleton evolution through Earth history. Indeed, extensive compilation of non-skeletal carbonates and hypercalcifying animals in the Phanerozoic reveals that the Mg/Ca and [Ca] of seawater during periods of aragonite or calcite-dominated seas had a strong influence on skeletal mineralogy (Stanley & Hardie, 1998; Stanley, 2006; Porter, 2010). High-Mg calcite and aragonite shells appear to have dominated under aragonite seas, while shells composed of low Mg calcite dominated under calcite seas. This pattern is also seen in the Cambrian Period when the first massive biodiversification of skeletal animals occured (Porter, 2007). In the terminal Ediacaran, the widespread appearance of seafloor aragonite fans (Grotzinger, 2000; Grotzinger *et al.*, 2005; Hall *et al.*, 2013) and rapid accumulation of carbonates supports the aragonite sea hypothesis, and is consistent with the inferred high-Mg calcite mineralogy of *Cloudina* (Grant, 1990; Zhuravlev *et al.*, 2012).

Temporal growth in the oceanic sulfate reservoir

Projected to the world stage and viewed through the long lens of Earth history, paired sulfur isotope data in the terminal Ediacaran Gaojiashan Member stand out among the highest $\delta^{34}S_{sulfate}$ values (up to +40‰) and largest S isotope fractionations (ca. +70‰) for the whole Precambrian (Fig. 9). This pattern may reflect a strongly stratified ocean (e.g., Jiang *et al.*, 2007; Shen *et al.*, 2008, 2010, 2011; Li *et al.*, 2010), which would be particularly meaningful during the terminal Ediacaran when a putative atmospheric

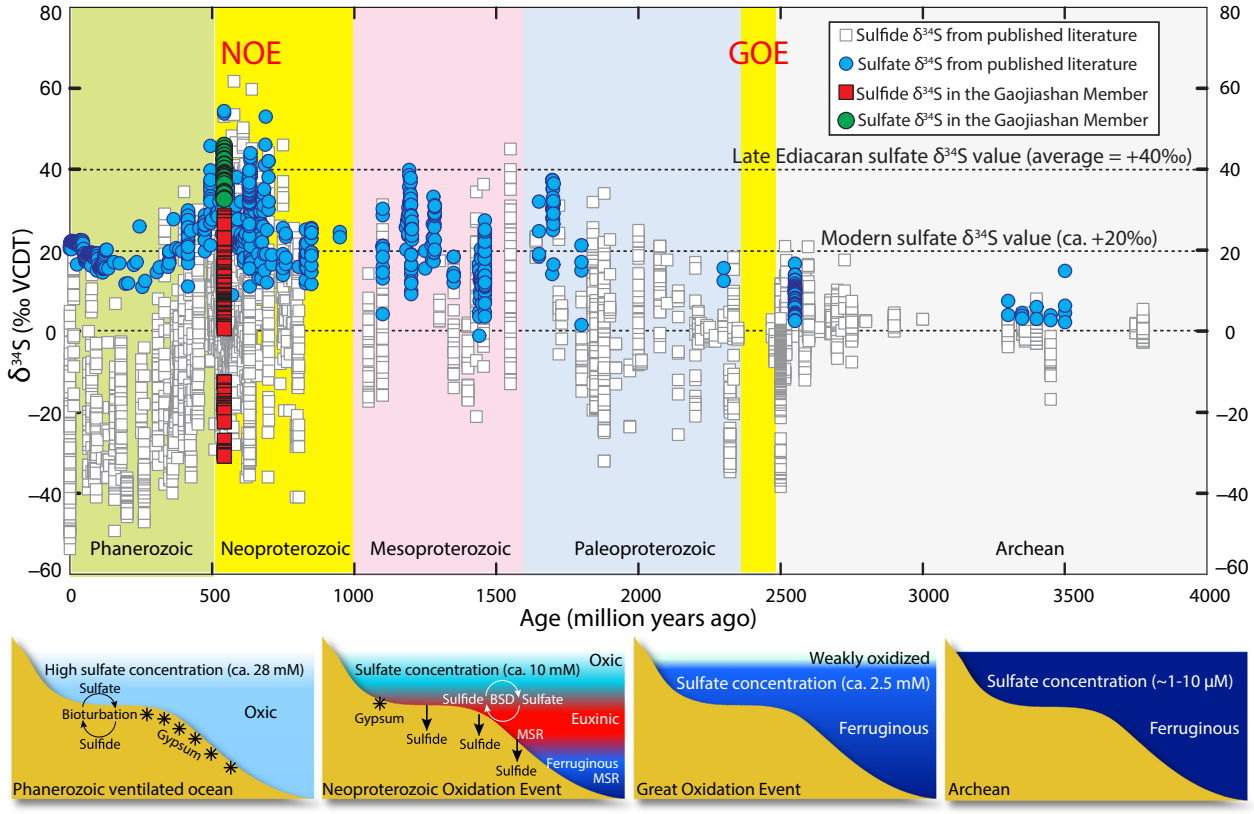

Fig. 9 Evaporite, CAS, and pyrite sulfur isotope data through Earth history. Paired $\delta^{34}S$ data are compiled from the literature [after (Canfield & Farquhar, 2009; Och & Shields-Zhou, 2012; Sahoo *et al.*, 2012)]. Recently published Neoarchean $\delta^{34}S$ data have also been included (e.g., Paris *et al.*, 2014; Zhelezinskaia *et al.*, 2014). The sulfate concentration constraints are ca. 1–10 μM during Archean (Habicht *et al.*, 2002; Zhelezinskaia *et al.*, 2014), ca. 2.5 mM after the GOE (Shen *et al.*, 2002; Canfield, 2004; Kah *et al.*, 2004; Hurtgen *et al.*, 2005; Bekker *et al.*, 2006; Canfield & Farquhar, 2009; Reuschel *et al.*, 2012), and ca. 10 mM during NOE (Canfield & Farquhar, 2009; Algeo *et al.*, 2015). $\delta^{34}S_{sulfate}$ composition of the terminal Ediacaran ocean (ca. +40‰) was determined by measurements of bedded evaporites in Oman (Fike & Grotzinger, 2008). GOE = Great Oxidation Event; NOE = Neoproterozoic Oxidation Event. The four conceptual biogeochemical models for redox architectures of the ocean during Archean, GOE, NOE, and Phanerozoic are shown in the panels beneath the time-series data. See the main text for detailed discussions.

and oceanic oxygenation event occurred (i.e., Neoproterozoic Oxygenation Event, or NOE) (Kaufman *et al.*, 1993; Shields-Zhou & Och, 2011; Och & Shields-Zhou, 2012; Lyons *et al.*, 2014; Liu *et al.*, 2016).

Growth of the Ediacaran sulfate pool has been hypothesized to be associated with the NOE (Fike *et al.*, 2006), which occurred in the aftermath of the Marinoan ice age (ca. 635 Ma). A recent quantitative model analysis based on sulfur isotope trends through the Ediacaran Period suggests that oceanic $[SO_4^{2-}]$ was low (<5 mM) in the aftermath of the Marinoan glaciation, but then rose (>5 mM) across the Ediacaran–Cambrian boundary (Algeo *et al.*, 2015). The inflection of sulfate concentrations may well have coincided with the middle Ediacaran Shuram excursion, a profound negative carbon isotope anomaly (Grotzinger *et al.*, 2011) recognized in multiple sections across the globe including Shuram Formation in Oman and the upper Doushantuo Formation of South China (Cui *et al.*, 2015). Sulfur isotope profiles in both regions reveal a parallel decrease in both $\delta^{34}S_{pyrite}$ and $\delta^{34}S_{CAS}$ (Cui *et al.*, 2015) that likely reflect the significant growth of the Ediacaran sulfate pool (Fike *et al.*, 2006; Halverson & Hurtgen, 2007; Kaufman *et al.*, 2007; McFadden *et al.*, 2008). Consistent with this view, psuedomorphs of gypsum are found in the Shuram equivalent Wonoka Formation in South Australia (Calver, 2000) and in the Doushantuo (Lu *et al.*, 2013). Above the Shuram, an increasing number of bedded evaporite horizons have been discovered in terminal Ediacaran successions, including the Dengying (Siegmund & Erdtmann, 1994; Duda *et al.*, 2015; and this study) and Ara formations (Fike & Grotzinger, 2010), as well as the Hanseran Evaporite Group in northwestern India (Strauss *et al.*, 2001; Mazumdar & Strauss, 2006).

The trigger for the terminal Ediacaran rise in seawater sulfate remains a question of considerable debate. It has been proposed by Canfield & Farquhar (2009) that the emergence of bioturbation near the Ediacaran–Cambrian boundary was the proximate cause insofar as sediment

mixing would result in enhanced sulfide oxidation and recycling (Bottjer *et al.*, 2000; Meysman *et al.*, 2006; Rogov *et al.*, 2012; Chen *et al.*, 2014). While bioturbation clearly modified ecosystems in the Fortunian Stage of the Cambrian Period (Bottjer *et al.*, 2000; Meysman *et al.*, 2006), there is little support for deep penetration by animals into sedimentary layers dominated by microbial mats in the Shuram or terminal Ediacaran intervals (e.g., Carbone & Narbonne, 2014; Meyer *et al.*, 2014). Moreover, recent investigations have demonstrated that the mixing of sediments on marine shelves remained limited until at least the late Silurian, 120 million years after the Precambrian–Cambrian transition (Tarhan & Droser, 2014; Gingras & Konhauser, 2015; Tarhan *et al.*, 2015).

Alternatively, it is likely that the increase in Ediacaran sulfate concentrations was driven by enhanced oxidative weathering of pyrite in continental and oceanic sediments exposed by sea level regression (Kaufman *et al.*, 2007; Wang *et al.*, 2016). This scenario is consistent with the profound increase in seawater $^{87}Sr/^{86}Sr$ (from ca. 0.7080 to 0.7090) recorded globally in carbonates deposited during the Shuram excursion (Burns *et al.*, 1994; Calver, 2000; Melezhik *et al.*, 2009; Sawaki *et al.*, 2010; Cui *et al.*, 2015). The Sr isotope shift most likely accompanied enhanced silicate weathering (Kaufman *et al.*, 1993; Halverson *et al.*, 2007; Cui *et al.*, 2015), which led to an increase in the delivery of nutrient and sulfate to the oceans. By stimulating photosynthesis, these continental fluxes would on the one hand result in the oxidation of surface environments, while on the other, the remineralization of organic matter along marginal marine settings would simultaneously resulted in the expansion of oxygen minimum zones (OMZs). Oceanic redox stratification would have simultaneously stimulated the oxidative side of the sulfur cycle through widespread sulfur disproportionation along chemoclines (Canfield & Thamdrup, 1994; Fike *et al.*, 2006; Wu *et al.*, 2015) and the reductive side through MSR within the anoxic plumes. Both microbial processes would have delivered ^{32}S sulfur as pyrite into the sediments and thereby drove oceanic sulfate compositions to positive $\delta^{34}S$ extremes (Canfield, 2004).

CONCLUSIONS

Terminal Ediacaran strata of the Gaojiashan Member preserve a record of dynamic carbon and sulfur cycling ultimately driven by tectonic forces, a rise in atmospheric oxygen, and enhanced chemical weathering of the exposed continents. Data from South China suggest that the attendant flux of nutrients and alkalinity increased oceanic productivity and carbonate saturation state, resulting in a redox stratified ocean basin where animals evolved to form calcareous shells, through the combined ecological pressure of predation and the environmental pressure of high carbonate saturation, for the first time in Earth history.

ACKNOWLEDGMENTS

We thank Rebecca Plummer, Mike Evans, and Brittney Gaeta for their assistance in the UMD Paleoclimate CoLaboratory. This research is funded by the NASA Exobiology grant (NNX12AR91G to AJK and NNX15AL27G to SX), the NSF Sedimentary Geology and Paleontology grant (EAR0844270 and EAR1528553 to AJK; EAR1528553 to SX), the NSF grant (EAR1032156) to the Arizona LaserChron Center, the AAPG Grants-In-Aid Program Marilyn Atwater Memorial Grant to HC, the Explorers Club Washington Group grant to HC, the Carnegie Institution of Washington Postdoctoral Fellowship to XML, and the National Natural Science Foundation of China grant (41572012) to YC. Thanks to the party chief of the Gaojiashan village Fazhi Li for his warm-hearted assistance in the field. Thanks to James Farquhar and Heather M. Stoll for helpful comments. The manuscript also benefits from constructive reviews by Pedro J. Marenco, Marc Laflamme, and an anonymous reviewer. Thanks also to the editor Kurt Konhauser for handling this manuscript.

REFERENCES

Algeo TJ, Luo GM, Song HY, Lyons TW, Canfield DE (2015) Reconstruction of secular variation in seawater sulfate concentrations. *Biogeosciences* **12**, 2131–2151.

Amthor JE, Grotzinger JP, Schröder S, Bowring SA, Ramezani J, Martin MW, Matter A (2003) Extinction of *Cloudina* and *Namacalathus* at the Precambrian-Cambrian boundary in Oman. *Geology* **31**, 431–434.

An Z, Jiang G, Tong J, Tian L, Ye Q, Song H, Song H (2015) Stratigraphic position of the Ediacaran Miaohe biota and its constrains on the age of the upper Doushantuo $\delta^{13}C$ anomaly in the Yangtze Gorges area, South China. *Precambrian Research* **271**, 243–253.

Bekker A, Karhu J, Kaufman A (2006) Carbon isotope record for the onset of the Lomagundi carbon isotope excursion in the Great Lakes area, North America. *Precambrian Research* **148**, 145–180.

Bengtson S, Zhao Y (1992) Predatorial borings in late Precambrian mineralized exoskeletons. *Science* **257**, 367–369.

Berner RA (2004) *The Phanerozoic Carbon Cycle: CO_2 and O_2*. Oxford University Press, New York.

Berner RA, Raiswell R (1983) Burial of organic carbon and pyrite sulfur in sediments over Phanerozoic time: a new theory. *Geochimica et Cosmochimica Acta* **47**, 855–862.

Berner RA, Raiswell R (1984) C/S method for distinguishing freshwater from marine sedimentary rocks. *Geology* **12**, 365–368.

Blättler CL, Jenkyns HC, Reynard LM, Henderson GM (2011) Significant increases in global weathering during Oceanic Anoxic Events 1a and 2 indicated by calcium isotopes. *Earth and Planetary Science Letters* **309**, 77–88.

Borowski WS, Paull CK, Ussler W (1996) Marine pore-water sulfate profiles indicate *in situ* methane flux from underlying gas hydrate. *Geology* **24**, 655–658.

Borowski WS, Rodriguez NM, Paull CK, Ussler W (2013) Are ^{34}S-enriched authigenic sulfide minerals a proxy for elevated

methane flux and gas hydrates in the geologic record? *Marine and Petroleum Geology* **43**, 381–395.
Bottjer DJ, Hagadorn JW, Dornbos SQ (2000) The Cambrian substrate revolution. *GSA Today* **10**, 1–7.
Bouougri E, Porada H (2007) Mat-related features from the Terminal Ediacaran Nudaus Formation, Nama Group, Namibia. In *Atlas of Microbial Mat Features Preserved within the Siliciclastic Rock Record* (eds Schieber J, Bose PK, Eriksson PG, Banerjee S, Sarkar S, Altermann W, Catuneanu O). Elsevier, Amsterdam, pp. 214–221.
Bradley AS, Leavitt WD, Schmidt M, Knoll AH, Girguis PR, Johnston DT (2016) Patterns of sulfur isotope fractionation during microbial sulfate reduction. *Geobiology* **14**, 91–101.
Brennan ST, Lowenstein TK, Horita J (2004) Seawater chemistry and the advent of biocalcification. *Geology* **32**, 473–476.
Bristow TF, Bonifacie M, Derkowski A, Eiler JM, Grotzinger JP (2011) A hydrothermal origin for isotopically anomalous cap dolostone cements from south China. *Nature* **474**, 68–71.
Brocks JJ, Love GD, Summons RE, Knoll AH, Logan GA, Bowden SA (2005) Biomarker evidence for green and purple sulphur bacteria in a stratified Palaeoproterozoic sea. *Nature* **437**, 866–870.
Burns SJ, Haudenschild U, Matter A (1994) The strontium isotopic composition of carbonates from the late Precambrian ($\sim$ 560-540 Ma) Huqf Group of Oman. *Chemical Geology* **111**, 269–282.
Butterfield N (2009) Oxygen, animals and oceanic ventilation: an alternative view. *Geobiology* **7**, 1–7.
Butterfield NJ (2011) Animals and the invention of the Phanerozoic Earth system. *Trends in Ecology & Evolution* **26**, 81–87.
Cai C, Hu W, Worden RH (2001) Thermochemical sulphate reduction in Cambro-Ordovician carbonates in Central Tarim. *Marine and Petroleum Geology* **18**, 729–741.
Cai C, Worden RH, Bottrell SH, Wang L, Yang C (2003) Thermochemical sulphate reduction and the generation of hydrogen sulphide and thiols (mercaptans) in Triassic carbonate reservoirs from the Sichuan Basin, China. *Chemical Geology* **202**, 39–57.
Cai C, Xie Z, Worden RH, Hu G, Wang L, He H (2004) Methane-dominated thermochemical sulphate reduction in the Triassic Feixianguan Formation East Sichuan Basin, China: towards prediction of fatal H_2S concentrations. *Marine and Petroleum Geology* **21**, 1265–1279.
Cai Y, Hua H, Xiao S, Schiffbauer JD, Li P (2010) Biostratinomy of the late Ediacaran pyritized Gaojiashan Lagerstätte from southern Shaanxi, South China: importance of event deposits. *Palaios* **25**, 487–506.
Cai Y, Schiffbauer JD, Hua H, Xiao S (2011) Morphology and paleoecology of the late Ediacaran tubular fossil *Conotubus hemiannulatus* from the Gaojiashan Lagerstätte of southern Shaanxi Province, South China. *Precambrian Research* **191**, 46–57.
Cai Y, Hua H, Schiffbauer JD, Sun B, Yuan X (2014) Tube growth patterns and microbial mat-related lifestyles in the Ediacaran fossil *Cloudina*, Gaojiashan Lagerstätte, South China. *Gondwana Research* **25**, 1008–1018.
Calver CR (2000) Isotope stratigraphy of the Ediacarian (Neoproterozoic III) of the Adelaide Rift Complex, Australia, and the overprint of water column stratification. *Precambrian Research* **100**, 121–150.
Canfield DE (2004) The evolution of the Earth surface sulfur reservoir. *American Journal of Science* **304**, 839–861.
Canfield DE, Farquhar J (2009) Animal evolution, bioturbation, and the sulfate concentration of the oceans. *Proceedings of the National Academy of Sciences of the United States of America* **106**, 8123–8127.
Canfield DE, Thamdrup B (1994) The production of ^{34}S-depleted sulfide during bacterial disproportionation of elemental sulfur. *Science* **266**, 1973–1975.
Canfield DE, Farquhar J, Zerkle AL (2010) High isotope fractionations during sulfate reduction in a low-sulfate euxinic ocean analog. *Geology* **38**, 415–418.
Carbone C, Narbonne GM (2014) When life got smart: the evolution of behavioral complexity through the Ediacaran and early Cambrian of NW Canada. *Journal of Paleontology* **88**, 309–330.
Chen Z, Zhou C, Meyer M, Xiang K, Schiffbauer JD, Yuan X, Xiao S (2013) Trace fossil evidence for Ediacaran bilaterian animals with complex behaviors. *Precambrian Research* **224**, 690–701.
Chen Z, Zhou C, Xiao S, Wang W, Guan C, Hua H, Yuan X (2014) New Ediacara fossils preserved in marine limestone and their ecological implications. *Scientific Reports* **4**, 4180.
Chen D, Zhou X, Fu Y, Wang J, Yan D (2015) New U-Pb zircon ages of the Ediacaran-Cambrian boundary strata in South China. *Terra Nova* **27**, 62–68.
Condon D, Zhu M, Bowring S, Wang W, Yang A, Jin Y (2005) U-Pb ages from the Neoproterozoic Doushantuo Formation, China. *Science* **308**, 95–98.
Conway Morris S, Mattes BW, Chen M (1990) The early skeletal organism *Cloudina*: new occurrences from Oman and possibly China. *American Journal of Science* **290-A**, 245–260.
Cortijo I, Martí Mus M, Jensen S, Palacios T (2010) A new species of *Cloudina* from the terminal Ediacaran of Spain. *Precambrian Research* **176**, 1–10.
Cortijo I, Cai Y, Hua H, Schiffbauer JD, Xiao S (2015) Life history and autecology of an Ediacaran index fossil: development and dispersal of *Cloudina*. *Gondwana Research* **28**, 419–424.
Cui H, Kaufman AJ, Xiao S, Zhu M, Zhou C, Liu X-M (2015) Redox architecture of an Ediacaran ocean margin: integrated chemostratigraphic ($\delta^{13}C$–$\delta^{34}S$–$^{87}Sr/^{86}Sr$–Ce/Ce*) correlation of the Doushantuo Formation, South China. *Chemical Geology* **405**, 48–62.
De La Rocha C, DePaolo DJ (2000) Isotopic evidence for variations in the marine calcium cycle over the Cenozoic. *Science* **289**, 1176–1178.
DePaolo DJ (2004) Calcium isotopic variations produced by biological, kinetic, radiogenic and nucleosynthetic processes. *Reviews in Mineralogy and Geochemistry* **55**, 255–288.
DePaolo DJ (2011) Surface kinetic model for isotopic and trace element fractionation during precipitation of calcite from aqueous solutions. *Geochimica et Cosmochimica Acta* **75**, 1039–1056.
Derry LA (2010) A burial diagenesis origin for the Ediacaran Shuram-Wonoka carbon isotope anomaly. *Earth and Planetary Science Letters* **294**, 152–162.
Des Marais DJ (1990) Microbial mats and the early evolution of life. *Trends in Ecology & Evolution* **5**, 140–144.
Duda J-P, Blumenberg M, Thiel V, Simon K, Zhu M, Reitner J (2014) Geobiology of a palaeoecosystem with Ediacara-type fossils: the Shibantan Member (Dengying Formation, South China). *Precambrian Research* **255**, 48–62.
Duda J-P, Zhu M, Reitner J (2015) Depositional dynamics of a bituminous carbonate facies in a tectonically induced intra-platform basin: the Shibantan Member (Dengying Formation, Ediacaran Period). *Carbonates Evaporites* **31**, 87–99.
Erwin DH (2015) A public goods approach to major evolutionary innovations. *Geobiology* **13**, 308–315.

Falkowski PG, Fenchel T, Delong EF (2008) The microbial engines that drive Earth's biogeochemical cycles. *Science* **320**, 1034–1039.
Fike DA, Grotzinger JP (2008) A paired sulfate-pyrite $\delta^{34}S$ approach to understanding the evolution of the Ediacaran-Cambrian sulfur cycle. *Geochimica et Cosmochimica Acta* **72**, 2636–2648.
Fike DA, Grotzinger JP (2010) A $\delta^{34}S_{SO4}$ approach to reconstructing biogenic pyrite burial in carbonate-evaporite basins: an example from the Ara Group, Sultanate of Oman. *Geology* **38**, 371–374.
Fike DA, Grotzinger JP, Pratt LM, Summons RE (2006) Oxidation of the Ediacaran ocean. *Nature* **444**, 744–747.
Fike DA, Gammon CL, Ziebis W, Orphan VJ (2008) Micron-scale mapping of sulfur cycling across the oxycline of a cyanobacterial mat: a paired nanoSIMS and CARD-FISH approach. *The ISME Journal* **2**, 749–759.
Fike DA, Finke N, Zha J, Blake G, Hoehler TM, Orphan VJ (2009) The effect of sulfate concentration on (sub) millimeter-scale sulfide $\delta^{34}S$ in hypersaline cyanobacterial mats over the diurnal cycle. *Geochimica et Cosmochimica Acta* **73**, 6187–6204.
Gaidos E, Dubuc T, Dunford M, McAndrew P, Padilla-GamiÑO J, Studer B, Weersing K, Stanley S (2007) The Precambrian emergence of animal life: a geobiological perspective. *Geobiology* **5**, 351–373.
Gaucher C, Germs GJB (2009) Skeletonised metazoans and protists. In *Developments in Precambrian Geology* (Gaucher C, Sial AN, Frimmel HE, Halverson GP). Elsevier, Amsterdam, pp. 327–338.
Gehling JG (1999) Microbial mats in terminal Proterozoic siliciclastics: Ediacaran death masks. *Palaios* **14**, 40–57.
Gehrels GE, Valencia VA, Ruiz J (2008) Enhanced precision, accuracy, efficiency, and spatial resolution of U-Pb ages by laser ablation–multicollector–inductively coupled plasma–mass spectrometry. *Geochemistry, Geophysics, Geosystems* **9**, Q03017.
Gill BC, Lyons TW, Frank TD (2008) Behavior of carbonate-associated sulfate during meteoric diagenesis and implications for the sulfur isotope paleoproxy. *Geochimica et Cosmochimica Acta* **72**, 4699–4711.
Gingras M, Konhauser K (2015) Digging deeper. *Nature Geoscience* **8**, 825–826.
Gomes ML, Hurtgen MT (2015) Sulfur isotope fractionation in modern euxinic systems: implications for paleoenvironmental reconstructions of paired sulfate–sulfide isotope records. *Geochimica et Cosmochimica Acta* **157**, 39–55.
Grant S (1990) Shell structure and distribution of *Cloudina*, a potential index fossil for the terminal Proterozoic. *American Journal of Science* **290**, 261–294.
Grant SWF (1992) Carbon isotopic vital effect and organic diagenesis, Lower Cambrian Forteau Formation, northwest Newfoundland: implications for $\delta^{13}C$ chemostratigraphy. *Geology* **20**, 243–246.
Grotzinger JP (2000) Facies and paleoenvironmental setting of thrombolite-stromatolite reefs, terminal Proterozoic Nama Group (ca. 550–543 Ma), central and southern Namibia. *Communications of the Geological Survey of Namibia* **12**, 251–264.
Grotzinger J, Adams E, Schröder S (2005) Microbial–metazoan reefs of the terminal Proterozoic Nama Group (c. 550–543 Ma), Namibia. *Geological Magazine* **142**, 499–517.
Grotzinger JP, Fike DA, Fischer WW (2011) Enigmatic origin of the largest-known carbon isotope excursion in Earth's history. *Nature Geoscience* **4**, 285–292.
Habicht KS, Canfield DE (2001) Isotope fractionation by sulfate-reducing natural populations and the isotopic composition of sulfide in marine sediments. *Geology* **29**, 555–558.
Habicht KS, Gade M, Thamdrup B, Berg P, Canfield DE (2002) Calibration of sulfate levels in the Archean ocean. *Science* **298**, 2372–2374.
Hall M, Kaufman AJ, Vickers-Rich P, Ivantsov A, Trusler P, Linnemann U, Hofmann M, Elliott D, Cui H, Fedonkin M, Hoffmann K-H, Wilson SA, Schneider G, Smith J (2013) Stratigraphy, palaeontology and geochemistry of the late Neoproterozoic Aar Member, southwest Namibia: reflecting environmental controls on Ediacara fossil preservation during the terminal Proterozoic in African Gondwana. *Precambrian Research* **238**, 214–232.
Halverson GP, Hurtgen MT (2007) Ediacaran growth of the marine sulfate reservoir. *Earth and Planetary Science Letters* **263**, 32–44.
Halverson GP, Dudás FÖ, Maloof AC, Bowring SA (2007) Evolution of the $^{87}Sr/^{86}Sr$ composition of Neoproterozoic seawater. *Palaeogeography, Palaeoclimatology, Palaeoecology* **256**, 103–129.
Hayes JM (1993) Factors controlling ^{13}C contents of sedimentary organic compounds: principles and evidence. *Marine Geology* **113**, 111–125.
Hayes JM, Kaplan IR, Wedeking KW (1983) Precambrian organic geochemistry-Preservation of the record. In *Earth's Earliest Biosphere: Its Origin and Evolution* (ed. Schopf JW). Princeton University Press, Princeton, NJ, pp. 93–134.
Higgins JA, Schrag DP (2003) Aftermath of a snowball Earth. *Geochemistry, Geophysics, Geosystems* **4**, 1028.
Higgins J, Fischer W, Schrag D (2009) Oxygenation of the ocean and sediments: consequences for the seafloor carbonate factory. *Earth and Planetary Science Letters* **284**, 25–33.
Hoffman PF, Schrag DP (2002) The snowball Earth hypothesis: testing the limits of global change. *Terra Nova* **14**, 129–155.
Houghton J, Fike D, Druschel G, Orphan V, Hoehler TM, Des Marais DJ (2014) Spatial variability in photosynthetic and heterotrophic activity drives localized $\delta^{13}C_{org}$ fluctuations and carbonate precipitation in hypersaline microbial mats. *Geobiology* **12**, 557–574.
Hua H, Pratt BR, Zhang L-Y (2003) Borings in *Cloudina* shells: complex predator-prey dynamics in the terminal Neoproterozoic. *Palaios* **18**, 454–459.
Hua H, Chen Z, Yuan X, Zhang L, Xiao S (2005) Skeletogenesis and asexual reproduction in the earliest biomineralizing animal Cloudina. *Geology* **33**, 277–280.
Hua H, Chen Z, Yuan X (2007) The advent of mineralized skeletons in Neoproterozoic Metazoa – new fossil evidence from the Gaojiashan Fauna. *Geological Journal* **42**, 263–279.
Hurtgen MT, Arthur MA, Halverson GP (2005) Neoproterozoic sulfur isotopes, the evolution of microbial sulfur species, and the burial efficiency of sulfide as sedimentary pyrite. *Geology* **33**, 41–44.
Jacobsen SB, Kaufman AJ (1999) The Sr, C and O isotopic evolution of Neoproterozoic seawater. *Chemical Geology* **161**, 37–57.
Jiang G, Kaufman AJ, Christie-Blick N, Zhang S, Wu H (2007) Carbon isotope variability across the Ediacaran Yangtze platform in South China: implications for a large surface-to-deep ocean $\delta^{13}C$ gradient. *Earth and Planetary Science Letters* **261**, 303–320.
Jiang G, Shi X, Zhang S, Wang Y, Xiao S (2011) Stratigraphy and paleogeography of the Ediacaran Doushantuo Formation (ca. 635–551 Ma) in South China. *Gondwana Research* **19**, 831–849.
Johnston DT, Wolfe-Simon F, Pearson A, Knoll AH (2009) Anoxygenic photosynthesis modulated Proterozoic oxygen and

sustained Earth's middle age. *Proceedings of the National Academy of Sciences of the United States of America* **106**, 16925–16929.
Jørgensen BB, Böttcher ME, Lüschen H, Neretin LN, Volkov II (2004) Anaerobic methane oxidation and a deep H_2S sink generate isotopically heavy sulfides in Black Sea sediments 1. *Geochimica et Cosmochimica Acta* **68**, 2095–2118.
Kah LC, Lyons TW, Frank TD (2004) Low marine sulphate and protracted oxygenation of the Proterozoic biosphere. *Nature* **431**, 834–838.
Katz A, Sass E, Starinsky A, Holland H (1972) Strontium behavior in the aragonite-calcite transformation: an experimental study at 40–98° C. *Geochimica et Cosmochimica Acta* **36**, 481–496.
Kaufman AJ (2005) The calibration of Ediacaran time. *Science* **308**, 59–60.
Kaufman AJ, Hayes JM, Knoll AH, Germs GJB (1991) Isotopic compositions of carbonates and organic carbon from upper Proterozoic successions in Namibia: stratigraphic variation and the effects of diagenesis and metamorphism. *Precambrian Research* **49**, 301–327.
Kaufman AJ, Jacobsen SB, Knoll AH (1993) The Vendian record of Sr and C isotopic variations in seawater: implications for tectonics and paleoclimate. *Earth and Planetary Science Letters* **120**, 409–430.
Kaufman AJ, Knoll AH, Narbonne GM (1997) Isotopes, ice ages, and terminal Proterozoic earth history. *Proceedings of the National Academy of Sciences of the United States of America* **94**, 6600–6605.
Kaufman AJ, Jiang G, Christie-Blick N, Banerjee D, Rai V (2006) Stable isotope record of the terminal Neoproterozoic Krol platform in the Lesser Himalayas of northern India. *Precambrian Research* **147**, 156–185.
Kaufman AJ, Corsetti FA, Varni MA (2007) The effect of rising atmospheric oxygen on carbon and sulfur isotope anomalies in the Neoproterozoic Johnnie Formation, Death Valley, USA. *Chemical Geology* **237**, 47–63.
Kempe S, Kazmierczak J, Degens ET (1989) The soda ocean concept and its bearing on biotic evolution. In *Origin, Evolution, and Modern Aspects of Biomineralization in Plants and Animals* (ed. Crick RE). Plenum Press, Springer, New York, pp. 29–43.
Knauth LP, Kennedy MJ (2009) The late Precambrian greening of the Earth. *Nature* **460**, 728–732.
Knoll AH (2003a) Biomineralization and evolutionary history. *Reviews in Mineralogy and Geochemistry* **54**, 329–356.
Knoll AH (2003b) The geological consequences of evolution. *Geobiology* **1**, 3–14.
Knoll AH, Fischer WW (2011) Skeletons and ocean chemistry: The long view. In *Ocean Acidification*. (ed Gattuso J-P, Hansson L). Oxford University Press, New York, pp. 67–82.
Kump L, Arthur M, Patzkowsky M, Gibbs M, Pinkus D, Sheehan P (1999) A weathering hypothesis for glaciation at high atmospheric pCO_2 during the Late Ordovician. *Palaeogeography, Palaeoclimatology, Palaeoecology* **152**, 173–187.
Leavitt WD (2014) On the mechanisms of sulfur isotope fractionation during microbial sulfate reduction. Dissertation.
Leavitt WD, Bradley AS, Halevy I, Johnston DT (2013) Influence of sulfate reduction rates on the Phanerozoic sulfur isotope record. *Proceedings of the National Academy of Sciences of the United States of America* **110**, 11244–11249.
Lenton TM, Boyle RA, Poulton SW, Shields-Zhou GA, Butterfield NJ (2014) Co-evolution of eukaryotes and ocean oxygenation in the Neoproterozoic era. *Nature Geoscience* **7**, 257–265.
Li C, Love GD, Lyons TW, Fike DA, Sessions AL, Chu X (2010) A stratified redox model for the Ediacaran ocean. *Science* **328**, 80–83.
Ling H-F, Chen X, Li D, Wang D, Shields-Zhou GA, Zhu M (2013) Cerium anomaly variations in Ediacaran–earliest Cambrian carbonates from the Yangtze Gorges area, South China: implications for oxygenation of coeval shallow seawater. *Precambrian Research* **225**, 110–127.
Liu X-M, Kah LC, Knoll AH, Cui H, Kaufman AJ, Shahar A, Hazen RM (2016) Tracing Earth's O_2 evolution using Zn/Fe ratios in marine carbonates. *Geochemical Perspectives Letters* **2**, 24–34.
Lorens RB (1981) Sr, Cd, Mn and Co distribution coefficients in calcite as a function of calcite precipitation rate. *Geochimica et Cosmochimica Acta* **45**, 553–561.
Loyd SJ, Marenco PJ, Hagadorn JW, Lyons TW, Kaufman AJ, Sour-Tovar F, Corsetti FA (2013) Local $\delta^{34}S$ variability in ~580 Ma carbonates of northwestern Mexico and the Neoproterozoic marine sulfate reservoir. *Precambrian Research* **224**, 551–569.
Lu M, Zhu M, Zhang J, Shields-Zhou G, Li G, Zhao F, Zhao X, Zhao M (2013) The DOUNCE event at the top of the Ediacaran Doushantuo Formation, South China: broad stratigraphic occurrence and non-diagenetic origin. *Precambrian Research* **225**, 86–109.
Ludwig K (2008) Isoplot 3.6, Berkeley Geochronology Center. Special Publication **4**, 77.
Lyons TW, Walter LM, Gellatly AM, Martini AM, Blake RE (2004) Sites of anomalous organic remineralization in the carbonate sediments of South Florida, USA: the sulfur cycle and carbonate-associated sulfate. *Geological Society of America Special Papers* **379**, 161–176.
Lyons TW, Reinhard CT, Planavsky NJ (2014) The rise of oxygen in Earth's early ocean and atmosphere. *Nature* **506**, 307–315.
Marenco PJ, Corsetti FA, Hammond DE, Kaufman AJ, Bottjer DJ (2008) Oxidation of pyrite during extraction of carbonate associated sulfate. *Chemical Geology* **247**, 124–132.
Martin AJ, Southworth S, Collins JC, Fisher SW, Kingman ER (2015) Laurentian and Amazonian sediment sources to Neoproterozoic–lower Paleozoic Maryland Piedmont rocks. *Geosphere* **11**, 1042–1061.
Mazumdar A, Strauss H (2006) Sulfur and strontium isotopic compositions of carbonate and evaporite rocks from the late Neoproterozoic–early Cambrian Bilara Group (Nagaur-Ganganagar Basin, India): constraints on intrabasinal correlation and global sulfur cycle. *Precambrian Research* **149**, 217–230.
McArthur J, Howarth R, Shields G (2012) Strontium isotope stratigraphy. In *A Geologic Time Scale* (ed. Gradstein FM, Ogg JG, Schmitz MD, Ogg GM). Elsevier B.V, Amsterdam, pp. 127–144.
McFadden KA, Huang J, Chu X, Jiang G, Kaufman AJ, Zhou C, Yuan X, Xiao S (2008) Pulsed oxidation and biological evolution in the Ediacaran Doushantuo Formation. *Proceedings of the National Academy of Sciences of the United States of America* **105**, 3197–3202.
Melezhik VA, Pokrovsky BG, Fallick AE, Kuznetsov AB, Bujakaite MI (2009) Constraints on $^{87}Sr/^{86}Sr$ of Late Ediacaran seawater: insight from Siberian high-Sr limestones. *Journal of the Geological Society* **166**, 183–191.
Meyer M, Schiffbauer DJ, Xiao S, Cai Y, Hua H (2012) Taphonomy of the upper Ediacaran enigmatic ribbonlike fossil *Shaanxilithes*. *Palaios* **27**, 354–372.

Meyer M, Xiao S, Gill BC, Schiffbauer JD, Chen Z, Zhou C, Yuan X (2014) Interactions between Ediacaran animals and microbial mats: insights from *Lamonte trevallis*, a new trace fossil from the Dengying Formation of South China. *Palaeogeography, Palaeoclimatology, Palaeoecology* **396**, 62–74.
Meysman FJ, Middelburg JJ, Heip CH (2006) Bioturbation: a fresh look at Darwin's last idea. *Trends in Ecology & Evolution* **21**, 688–695.
Narbonne GM, Laflamme M, Trusler PW, Dalrymple RW, Greentree C (2014) Deep-water Ediacaran fossils from northwestern Canada: taphonomy, ecology, and evolution. *Journal of Paleontology* **88**, 207–223.
Nielsen LC, Druhan JL, Yang W, Brown ST, DePaolo DJ (2011) Calcium isotopes as tracers of biogeochemical processes. In *Handbook of Environmental Isotope Geochemistry* (ed. Baskaran M). Springer-Verlag, Berlin, pp. 105–124.
Och LM, Shields-Zhou GA (2012) The Neoproterozoic oxygenation event: environmental perturbations and biogeochemical cycling. *Earth-Science Reviews* **110**, 26–57.
Paris G, Adkins J, Sessions A, Webb S, Fischer W (2014) Neoarchean carbonate–associated sulfate records positive $\Delta^{33}S$ anomalies. *Science* **346**, 739–741.
Peng Y, Bao H, Pratt LM, Kaufman AJ, Jiang G, Boyd D, Wang Q, Zhou C, Yuan X, Xiao S, Loyd S (2014) Widespread contamination of carbonate-associated sulfate by present-day secondary atmospheric sulfate: evidence from triple oxygen isotopes. *Geology* **42**, 815–818.
Penny A, Wood R, Curtis A, Bowyer F, Tostevin R, Hoffman K-H (2014) Ediacaran metazoan reefs from the Nama Group, Namibia. *Science* **344**, 1504–1506.
Porter SM (2007) Seawater chemistry and early carbonate biomineralization. *Science* **316**, 1302–1302.
Porter SM (2010) Calcite and aragonite seas and the *de novo* acquisition of carbonate skeletons. *Geobiology* **8**, 256–277.
Porter S (2011) The rise of predators. *Geology* **39**, 607–608.
Reuschel M, Melezhik V, Whitehouse M, Lepland A, Fallick A, Strauss H (2012) Isotopic evidence for a sizeable seawater sulfate reservoir at 2.1 Ga. *Precambrian Research* **192**, 78–88.
Ries JB, Fike DA, Pratt LM, Lyons TW, Grotzinger JP (2009) Superheavy pyrite (δ34Spyr>δ34SCAS) in the terminal Proterozoic Nama Group, southern Namibia: a consequence of low seawater sulfate at the dawn of animal life. *Geology* **37**, 743–746.
Rogov V, Marusin V, Bykova N, Goy Y, Nagovitsin K, Kochnev B, Karlova G, Grazhdankin D (2012) The oldest evidence of bioturbation on Earth. *Geology* **40**, 395–398.
Sahoo SK, Planavsky NJ, Kendall B, Wang X, Shi X, Scott C, Anbar AD, Lyons TW, Jiang G (2012) Ocean oxygenation in the wake of the Marinoan glaciation. *Nature* **489**, 546–549.
Sawaki Y, Ohno T, Tahata M, Komiya T, Hirata T, Maruyama S, Windley BF, Han J, Shu D, Li Y (2010) The Ediacaran radiogenic Sr isotope excursion in the Doushantuo Formation in the Three Gorges area, South China. *Precambrian Research* **176**, 46–64.
Sawaki Y, Tahata M, Ohno T, Komiya T, Hirata T, Maruyama S, Han J, Shu D (2014) The anomalous Ca cycle in the Ediacaran ocean: evidence from Ca isotopes preserved in carbonates in the Three Gorges area, South China. *Gondwana Research* **25**, 1070–1089.
Saylor BZ, Kaufman AJ, Grotzinger JP, Urban F (1998) A composite reference section for terminal Proterozoic strata of southern Namibia. *Journal of Sedimentary Research* **68**, 1223–1235.
Schiffbauer JD, Xiao S, Cai Y, Wallace AF, Hua H, Hunter J, Xu H, Peng Y, Kaufman AJ (2014) A unifying model for Neoproterozoic-Palaeozoic exceptional fossil preservation through pyritization and carbonaceous compression. *Nature Communications* **5**, 5754.
Schobben M, Stebbins A, Ghaderi A, Strauss H, Korn D, Korte C (2015) Flourishing ocean drives the end-Permian marine mass extinction. *Proceedings of the National Academy of Sciences of the United States of America* **112**, 10298–10303.
Schrag DP, Higgins JA, Macdonald FA, Johnston DT (2013) Authigenic carbonate and the history of the global carbon cycle. *Science* **339**, 540–543.
Shen Y, Canfield DE, Knoll AH (2002) Middle Proterozoic ocean chemistry: evidence from the McArthur Basin, northern Australia. *American Journal of Science* **302**, 81–109.
Shen B, Xiao S, Kaufman AJ, Bao H, Zhou C, Wang H (2008) Stratification and mixing of a post-glacial Neoproterozoic ocean: evidence from carbon and sulfur isotopes in a cap dolostone from northwest China. *Earth and Planetary Science Letters* **265**, 209–228.
Shen B, Xiao S, Zhou C, Kaufman AJ, Yuan X (2010) Carbon and sulfur isotope chemostratigraphy of the Neoproterozoic Quanji Group of the Chaidam Basin, NW China: basin stratification in the aftermath of an Ediacaran glaciation postdating the Shuram event? *Precambrian Research* **177**, 241–252.
Shen B, Xiao S, Bao H, Kaufman AJ, Zhou C, Yuan X (2011) Carbon, sulfur, and oxygen isotope evidence for a strong depth gradient and oceanic oxidation after the Ediacaran Hankalchough glaciation. *Geochimica et Cosmochimica Acta* **75**, 1357–1373.
Shields G (2007) A normalised seawater strontium isotope curve: possible implications for Neoproterozoic-Cambrian weathering rates and the further oxygenation of the Earth. *eEarth* **2**, 35–42.
Shields-Zhou G, Och L (2011) The case for a Neoproterozoic oxygenation event: geochemical evidence and biological consequences. *GSA Today* **21**, 4–11.
Siegmund H, Erdtmann B-D (1994) Facies and diagenesis of some upper proterozoic dolomites of South China. *Facies* **31**, 255–263.
Sim MS, Bosak T, Ono S (2011) Large sulfur isotope fractionation does not require disproportionation. *Science* **333**, 74–77.
Simkiss K (1977) Biomineralization and detoxification. *Calcified Tissue Research* **24**, 199–200.
Simkiss K (1989) Biomineralisation in the context of geological time. *Transactions of the Royal Society of Edinburgh: Earth Sciences* **80**, 193–199.
Sour-Tovar F, Hagadorn JW, Huitron-Rubio T (2007) Ediacaran and Cambrian index fossils from Sonora, Mexico. *Palaeontology* **50**, 169–175.
Stanley SM (2006) Influence of seawater chemistry on biomineralization throughout Phanerozoic time: Paleontological and experimental evidence. *Palaeogeography, Palaeoclimatology, Palaeoecology* **232**, 214–236.
Stanley SM, Hardie LA (1998) Secular oscillations in the carbonate mineralogy of reef-building and sediment-producing organisms driven by tectonically forced shifts in seawater chemistry. *Palaeogeography, Palaeoclimatology, Palaeoecology* **144**, 3–19.
Steiner M, Li G, Qian Y, Zhu M (2004) Lower Cambrian small shelly fossils of northern Sichuan and southern Shaanxi (China), and their biostratigraphic importance. *Geobios* **37**, 259–275.
Stoll HM, Bains S (2003) Coccolith Sr/Ca records of productivity during the Paleocene-Eocene thermal maximum from the Weddell Sea. *Paleoceanography* **18**, 1049.

Stoll HM, Schrag DP (2001) Sr/Ca variations in Cretaceous carbonates: relation to productivity and sea level changes. *Palaeogeography, Palaeoclimatology, Palaeoecology* **168**, 311–336.

Strauss H, Banerjee DM, Kumar V (2001) The sulfur isotopic composition of Neoproterozoic to early Cambrian seawater – evidence from the cyclic Hanseran evaporites, NW India. *Chemical Geology* **175**, 17–28.

Tang J, Köhler SJ, Dietzel M (2008) Sr^{2+}/Ca^{2+} and $^{44}Ca/^{40}Ca$ fractionation during inorganic calcite formation: I. Sr incorporation. *Geochimica et Cosmochimica Acta* **72**, 3718–3732.

Tarhan LG, Droser ML (2014) Widespread delayed mixing in early to middle Cambrian marine shelfal settings. *Palaeogeography, Palaeoclimatology, Palaeoecology* **399**, 310–322.

Tarhan LG, Droser ML, Planavsky NJ, Johnston DT (2015) Protracted development of bioturbation through the early Palaeozoic Era. *Nature Geoscience* **8**, 865–869.

Tesoriero AJ, Pankow JF (1996) Solid solution partitioning of Sr^{2+}, Ba^{2+}, and Cd^{2+} to calcite. *Geochimica et Cosmochimica Acta* **60**, 1053–1063.

Wang X, Jiang G, Shi X, Xiao S (2016) Paired carbonate and organic carbon isotope variations of the Ediacaran Doushantuo Formation from an upper slope section at Siduping, South China. *Precambrian Research* **273**, 53–66.

Weiner S, Dove PM (2003) An overview of biomineralization processes and the problem of the vital effect. *Reviews in Mineralogy and Geochemistry* **54**, 1–29.

Wing BA, Halevy I (2014) Intracellular metabolite levels shape sulfur isotope fractionation during microbial sulfate respiration. *Proceedings of the National Academy of Sciences of the United States of America* **111**, 18116–18125.

Wood R, Curtis A (2015) Extensive metazoan reefs from the Ediacaran Nama Group, Namibia: the rise of benthic suspension feeding. *Geobiology* **13**, 112–122.

Wood RA, Poulton SW, Prave AR, Hoffmann KH, Clarkson MO, Guilbaud R, Lyne JW, Tostevin R, Bowyer F, Penny AM, Curtis A, Kasemann SA (2015) Dynamic redox conditions control late Ediacaran metazoan ecosystems in the Nama Group, Namibia. *Precambrian Research* **261**, 252–271.

Wotte T, Shields-Zhou GA, Strauss H (2012) Carbonate-associated sulfate: experimental comparisons of common extraction methods and recommendations toward a standard analytical protocol. *Chemical Geology* **326–327**, 132–144.

Wray JL, Daniels F (1957) Precipitation of calcite and aragonite. *Journal of the American Chemical Society* **79**, 2031–2034.

Wu N, Farquhar J (2013) Metabolic rates and sulfur cycling in the geologic record. *Proceedings of the National Academy of Sciences of the United States of America* **110**, 11217–11218.

Wu N, Farquhar J, Fike DA (2015) Ediacaran sulfur cycle: Insights from sulfur isotope measurements ($\Delta^{33}S$ and $\delta^{34}S$) on paired sulfate–pyrite in the Huqf Supergroup of Oman. *Geochimica et Cosmochimica Acta* **164**, 352–364.

Xiao S (2014) Oxygen and early animal evolution. In *Treatise on Geochemistry*, 2nd edn. (eds Holland HD, Turekian KK). Elsevier, Oxford, Vol. 6, pp. 231–250.

Xiao S, Schiffbauer JD, McFadden KA, Hunter J (2010) Petrographic and SIMS pyrite sulfur isotope analyses of Ediacaran chert nodules: implications for microbial processes in pyrite rim formation, silicification, and exceptional fossil preservation. *Earth and Planetary Science Letters* **297**, 481–495.

Zhang F, Kendall B, Cui H, Anbar AD, Xiao S, Kaufman AJ (2015) An episode of widespread ocean anoxia during the latest Ediacaran Period revealed by light U isotope compositions in carbonates. GSA abstract.

Zhelezinskaia I, Kaufman AJ, Farquhar J, Cliff J (2014) Large sulfur isotope fractionations associated with Neoarchean microbial sulfate reduction. *Science* **346**, 742–744.

Zhou C, Xiao S (2007) Ediacaran $\delta^{13}C$ chemostratigraphy of South China. *Chemical Geology* **237**, 89–108.

Zhu M, Zhang J, Yang A (2007) Integrated Ediacaran (Sinian) chronostratigraphy of South China. *Palaeogeography, Palaeoclimatology, Palaeoecology* **254**, 7–61.

Zhuravlev AY, Liñán E, Vintaned JAG, Debrenne F, Fedorov AB (2012) New finds of skeletal fossils in the terminal Neoproterozoic of the Siberian Platform and Spain. *Acta Palaeontologica Polonica* **57**, 205–224.

Zhuravlev AY, Wood RA, Penny AM (2015) Ediacaran skeletal metazoan interpreted as a lophophorate. *Proceedings of the Royal Society of London B: Biological Sciences* **282**, 20151860.

SUPPORTING INFORMATION

Additional Supporting Information may be found in the online version of this article:

Table S1. U-Pb geochronologic analyses of two detrital zircon samples in the lower Gaojiashan Member.

Table S2. Chemostratigraphic data of carbonate C isotopes of the Doushantuo and Dengying formations plotted in Fig. 1.

Table S3. Chemostratigraphic data of C, O, and S isotopes of the Gaojiashan Member.

Table S4. Chemostratigraphic data of major and trace element concentrations of the Gaojiashan Member.

Fig. S1. Chemostratigraphic profiles for the Gaojiashan Member.